Master's Thesis

Rocking instability of rigid blocks atop a small pedestal

submitted in satisfaction of the requirements for the degree of
Diplom-Ingenieur
of the TU Wien, Faculty of Civil Engineering

Diplomarbeit

Schaukelinstabilität starrer Blöcke auf einem kleinen Podest

ausgeführt zum Zwecke der Erlangung des akademischen Grades eines
Diplom-Ingenieurs
eingereicht an der Technischen Universität Wien, Fakultät für Bauingenieurwesen

von

Dusan Radovic, BSc

Matr.Nr.: 01028202

unter der Anleitung von

Univ.Prof. Dipl.-Ing. Dr.techn. **Andreas Kolbitsch**

Dipl.-Ing. Dr.-Ing. **Andreas Rudisch**, BSc

Institut für Hochbau, Baudynamik und Gebaüdetechnik
Technische Universität Wien
Karlsplatz 13/208-02, 1040 Wien, Österreich

Wien, im März 2019 _____

Acknowledgments

I would like to express special thanks with a sense gratitude and respect to all those who supported me during my studies. First and foremost, I would like to thank my advisor Prof. Kolbitsch, who made it possible to do this work.

The constant efforts of Dr. Rudisch to help me with any problem, as well as his constrictive advises are highly appreciated.

I also want to thank my friends and colleges for their support, occasional proofreading and great friendship.

Special thanks goes to my family for all their support, immeasurable love as well as, patience and understanding from the first to the last day of my studies.I will always owe them for all their sacrifice and effort to shape me as a person I am today.

Abstract

While most studies in civil engineering, which deal with earthquakes, are directed toward the behavior of structural elements, significantly fewer deal with the instability of unattached or freestanding structures subjected to seismic excitation. These structures are however, highly susceptible to damage during moderate or strong earthquakes, as evidenced during numerous past events. In the context of this thesis these structures are statues atop a pedestal, hospital equipment, as well as numerous mechanical and electrical equipment, which provide services to the building. This thesis deals with these unattached, freestanding dual-body structures, modeled with two rigid blocks stocked one atop of the other. The aim of the thesis is to determine the influence of the statue geometry and slenderness, and the presence of the pedestal on the rocking vulnerability of such structures.

The motion of the freestanding, unattached structures, subjected to seismic excitation in all directions, is combination of rotating, sliding and jumping. Each response state is governed with a set of highly non-linear differential equations. The number of governing differential equations of motion increase exponentially when these objects are placed in stacked combination. To study all patterns combined would be desirable, but with so many components it is beyond the scope this thesis. Therefore, this thesis focuses on the response of rigid bodies with friction coefficients, in their base and between bodies, large enough so that any other motion except rocking is excluded. This may represent the worst case scenario for many fragile object (e.g. vases in a museum, historical statues) or for objects that may experience mechanical damage in critical components (e.g. medical equipment, servers). With this restriction, system behavior can be described in terms of four possible patterns, where the equations describing the rocking response are derived for each pattern.

This thesis also details a shake table test, in which the seismic response of a pair of wooden, unattached blocks was evaluated. The system consisted of a top block (statue) and a lower block (pedestal). The experiment was designed in such a way, that only rocking is allowed. Experimental variables included geometry of the top body, input motion, as well as presence of the pedestal.Three different statues were subjected to twelve input motions. Namely, four input motions corresponding to the earthquakes 1976 Friuli, 1995 Kobe, 1986 Loma Prieta, and 1994 Northridge, and input motions derived from these earthquakes were used. Furthermore, blocks were tested both in a stacked configuration and as a single body, allowing deeper understanding of the effect of the pedestal. Maximum acceleration that leads to overturning was determined in every test.

Kurzfassung

Während sich die meisten Studien, die sich mit Erdbeben befassen, auf das Verhalten von strukturellen Bauteilen eingehen, gehen wenige auf die Instabilität von nicht befestigten oder freistehenden Bauteilen, die den Erdbeben ausgesetzt sind, ein. Solche Strukturen sind bei moderaten oder starken Erdbeben sehr anfällig für Schäden, wie zahlreiche Ereignisse in der Vergangenheit gezeigt haben. Diese Diplomarbeit behandelt Statuen auf einem Podest, Krankenhausgeräte, sowie zahlreiche mechanische und elektrische Geräte, die für die Nutzung von Gebäuden notwendig sind. Diese nicht befestigte, freistehende Zweikörperstrukturen wurden in dieser Diplomarbeit mit zwei starren übereinander angeordneten Blöcken modelliert. Ziel der Diplomarbeit war es, den Einfluss der Statuengeometrie und Schlankheit sowie das Vorhandensein des Sockels auf die Schwinganfälligkeit solcher Strukturen zu bestimmen.

Die Bewegung der freistehenden, nicht befestigten Strukturen, die in alle Richtungen einer seismischen Erregung ausgesetzt sind, ist eine Kombination aus Rotieren, Gleiten und Kippen. Jeder Antwortzustand wird mit einem System stark nichtlinearer Differentialgleichungen geregelt. Die Anzahl den herrschenden Bewegungsdifferentialgleichungen nimmt exponentiell zu, wenn diese Strukturen in einer gestapelten Weise angeordnet werden. Es wäre wünschenswert, diese zusammen zu untersuchen, aber mit so vielen Komponenten würde es den Rahmen dieser Diplomarbeit sprengen.

Daher konzentriert sich diese Arbeit auf die Reaktion von starren Körpern, die große Reibungskoeffizienten in ihrer Basis und zwischen Körpern haben, um jegliche andere Bewegung außer dem Kippen auszuschließen. Dies kann das ungünstigste Szenario für viele fragile Objekte (z.B. Vase in einem Museum, historische Statuen) oder für solche, bei denen in kritischen Komponenten (z.B. medizinische Geräte, Server) mechanische Schäden auftreten können, sein. Mit dieser Einschränkung kann das Systemverhalten anhand von vier möglichen Mustern beschrieben werden.

In dieser Arbeit wird ein Versuch beschrieben, bei dem die seismische Reaktion eines Paares unverbundener Holzblöcke untersucht wurde. Das System bestand aus dem oberen Block (Statue) und dem Unteren (Podest). Der Versuch wurde so aufgebaut, dass nur Kippen erlaubt war. Zu den experimentellen Variablen gehörten die Geometrie des Oberkörpers, die Eingangsbewegung, sowie das Vorhandensein des Podests. Drei verschiedene Statuen wurden vier historischen Erdbeben (1976 Friuli, 1995 Kobe, 1986 Loma Prieta und 1994 Northridge) ausgesetzt. Darüber hinaus wurden die Statuen sowohl mit als auch ohne Podest getestet, um ein tieferes Verständnis der Wirkung des Podests zu ermöglichen. In jedem Experiment wurde die maximale Beschleunigung ermittelt, die zum Umstürzen führt.

Contents

Chapter 1

Introduction

An earthquake can cause priceless losses to cultural heritage, interruptions in business associated with loss of market share valuable electronic data, large economical losses, wide spread injuries, and even human fatalities. One major contributor to losses due to an earthquake are damages to non-structural components. These losses refer to architectural components, mechanical/electrical/plumbing (MEP) components and furniture, fixtures and equipment (FF&E) (Table 1.1).

The overturning of tall shelves with heavy storage items, articles falling overhead can injure residents of buildings or even be fatal. They can also become obstacles making it difficult or impossible for occupants to exit the building affected. Further, damages to electrical and other equipment can cause problems with functionality of buildings that are crucial to post-earthquake recovery, for example hospitals. In case of a earthquake medical equipment can overturn and suffer damages. As a result, the hospitals ability to fully function can be impaired. On the other hand overturning of statues and museum artifacts can damage them and result in the loss of precious cultural heritage items. Also, the classical temples located all over Mediterranean, which is seismically very active area, represent the cultural heritage important not only for the one nation but for the whole mankind. Columns of these temples are typically made of stone or marble blocks, called drums, resting atop of each other, with no connection. Due to their slenderness they are considered very susceptible to overturning, which is demonstrated in earthquake events through the history. From most of them, only what is left standing are single free-standing columns or small groups of columns connected through the epistyle. Two examples of such temples are shown in Figure 1.1.

While the statistical cost data for the non-structural damages is limited, it is widely agreed and reported that the total economic effect of all non-structural damages in earthquakes combined generally exceed those of structural damages [1]. Taking all this into consideration, it is very important to know the real dynamic behavior of non-structural components, in order to help in disaster mitigation. These considerations are the main motivation for this study. This is even more important in countries that are exposed to mid-intensity earthquakes, because in the case of moderate shaking buildings will not be at risk of collapsing, but non-structural components could be severely damaged. An example of such event is the Seebenstein earthquake which occurred in 1972 in Austria. Although the earthquake was not strong enough to produce large structural

damages, it caused damages to non-structural components. One such example is that 20m of balustrade on Vienna University collapsed as shown in Figure 1.2a.

Tab. 1.1: Non-structural components

Categories	Examples
Architectural Components	Partitions, false ceilings, storefronts, glazing, cladding, parapets, chimneys
Mechanical/Electrical/Plumbing (MEP) Components	Pumps, fans, air handling units, motors, boilers, transformers, ductwork and conduit, piping and plumbing
Furniture, Fixtures and equipment (FF&E) and content	Shelving, industrial storage racks, heavy items on racks, retail merchandise, computers and TVs, chemicals or hazardous materials, artifacts, statues and other free-standing objects

Some types of the non-structural components could simply be anchored, which would prevent them from moving during moderate or strong earthquake. This would make them more resistant to damage. However, there are many freestanding, non-structural components that simply can not be anchored. Examples of these objects are:

- Hospital equipment that can't be anchored (large coolers to store medicine, patient monitoring monitoring equipment, patient treatment equipment)
- Laboratory supplies and equipment (chemicals being stored in glass containers next to each other on shelves where they can overturn, break and mix, which can be very dangerous)
- Servers which are prone to rocking
- Personal computers and communication equipment important for post earthquake recovery
- Statues, many of them standing on a pedestal, which have precious cultural significance

These unattached, freestanding structures are prone to rocking and overturning. Thus they are highly vulnerable to damage in case of an earthquake, as observed in numerous post earthquake field investigations. Some examples can be found in Figure 1.2.

This thesis deals with such structures and their dynamical behavior, represented by a rigid block atop a pedestal. Only symmetric, rigid bodies undergoing horizontal acceleration are considered. Further, assumption of the rigid foundation and infinite friction was made, as well as the point contact during impact. In this way the only possible response state is rocking about the corners of the blocks. The blocks are tested both in stacked combination as well as single blocks. It allows not only investigation of a dual-body system, but also the influence of the pedestal on the system. In this chapter motivation, as well as literature review is presented.

Chapter 2 gives the theory of the rocking blocks. Namely, in section 2.1 dynamic behavior of a single rigid block is examined. The equations for initiation of motion as well as those governing

the rocking motion are derived. Further, section 2.2 discusses the dynamic behavior of two blocks, where one is symmetrically placed atop of other. All different patterns of motion are categorized and criteria for initiation of motion are formulated. For each pattern, governing non-linear equations of motion as well as transition criteria between patterns, both with impact and in absence of it, are given.

Chapter 3 describes in detail the test program included in this study, including characteristics of experimental specimens and used instrumentation. In Chapter 4 the results of the experiment are discussed, and finally, the conclusion and future work is presented in Chapter 5.

(a) **(b)**

Fig. 1.1: View of: (a) the temple of Athena at Aegina [2]; (b) the temple of Zeus at Nemea [3] (both located in Greece)

The motion of the freestanding, unattached structures, subjected to seismic excitation in all directions, is a combination of rotating, sliding and jumping. In fact, there are six states [4]: rest, slide, rotation, slide-rotation, translation-jump and rotation-jump. Each of these states is governed with a set of highly non-linear differential equations. The number of governing differential equations of motion increase exponentially when these objects are placed in a stacked combination. To study those all together would be desirable, but with so many components, it would jump out of the frame of this thesis. Therefore, this thesis will focus on the response of rigid bodies with friction coefficients in their base and between bodies, large enough so that any other motion except rocking is excluded.

Rocking motion is dynamical process when a rigid body instantly changes its center of rotation from one point to another. It has been studied for a long time. In the late 19th century, Milne [5] and Perry [6] pioneered studies on the rocking of the free-standing rigid bodies However, the first systematic study on the dynamics of rigid body supported on a base undergoing horizontal acceleration was presented by Housner [7] and is know as *classical theory*. Housner examined the free- and forced-vibration response to single square and sine pulses excitation. Using an energy

approach, he obtained the equation for the period of the system, which is amplitude dependent. The author also found an expression to calculate the minimum acceleration required to overturn a single rigid body [7].

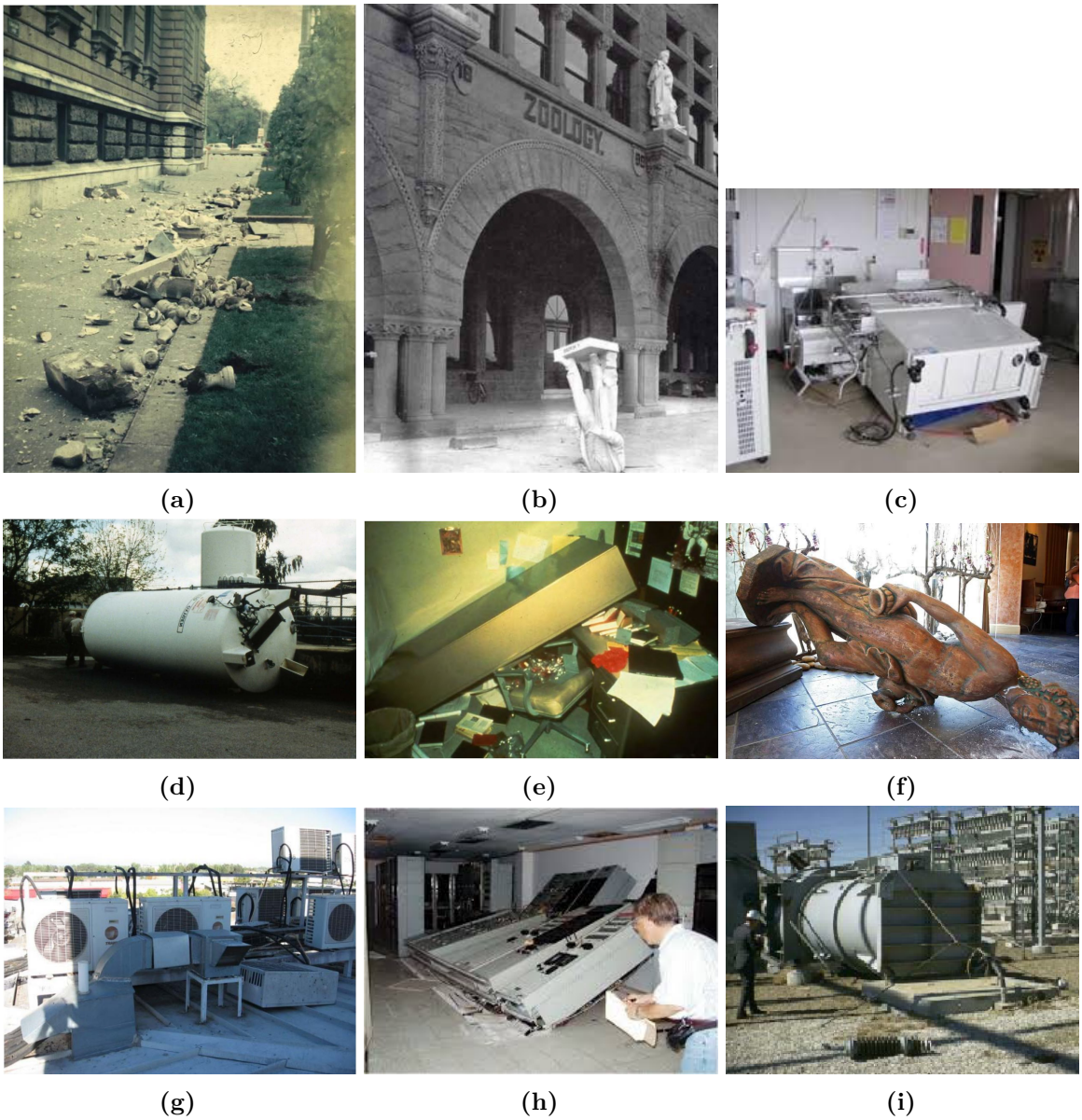

Fig. 1.2: Examples of earthquake damage to freestanding structures: (a) fallen balustrade on Vienna University-1972 Seebenstein earthquake (Photo/Walter Eppensteiner) [8], (b) the Agassiz statue-Stanford's 1906 earthquake (Photo/Frank Davey) [9], (c) overturned lab workstation-2011 Japan Earthquake [10], (d) toppled vertical tank, 1994 Northridge earthquake (Photo/OSHPD) [11], (e) overturned bookcase onto desk-1971 San Fernando earthquake [11], (f) overturned Statue fo Bachuss, a Roman god of wine inside the Ceja Vineyards tasting room-2014 South Napa earthquake (Photo/Reuters) [12], (g) roof top units-2010 Chile earthquake [11], (h) overturned equipment-1985 Mexico earthquake [11], (i) toppled electrical equipment-1971 Sylmar earthquake [13]

The response of a rigid block in free and forced rocking behavior, subjected to horizontal and vertical ground acceleration was tested by Aslam et al. [14]. He compared the experimental results with analytical results derived using the classical rocking model, and noted that the classical model was unable to accurately predict the response of the block. However, a relatively good match was found between model with the modified value of the coefficient of restitution.

In 1980, Yim et al. numerically integrated the piecewise equations of motion of the the model introduced by Housner and stated that the rocking response of unattached blocks was very sensitive to small changes in size and slenderness or input ground motion [15].

In the same year, Priestley et al. [16] experimentally tested a slender structure in an effort to validate some of the Housner's theoretical results. In their study they assumed that "it is possible to represent rocking block as a single degree-of-freedom (SDOF) oscillator, with constant damping, whose period depends on the amplitude of rocking." Under this assumption they used standard displacement and acceleration response spectra in order to establish a practical method to measure displacement of the center of gravity of the structure due to rocking motion.

Ishiyama [4] experimentally studied rectangular, symmetric, rigid bodies subjected to harmonic ground motion for many frequencies and peak intensities. Rigid foundation was assumed, along with non-zero coefficient of restitution and possible sliding. Further, it was assumed that the interfaces are perfectly horizontal. Ishiyama analyzed impact from a rock, slide-rock and free-flight mode, and derived the equations of motion for six possible response states [4].

An investigation of the rocking response of a rigid body with harmonic input was conducted by Spanos and Koh [17]. Under assumption of infinite coefficient of friction, and in order to identify likely steady-state patterns of response, the linear and nonlinear equations of motion were solved numerically assuming zero initial conditions.

Furthermore, Tsao and Wong [18] investigated the rocking response both analytically and experimentally. They studied how various system parameters affect steady-state response and found good correlation between the experimental and analytical results.

In 1990, Hogan [19] studied the existence and stability of single-subharmonic responses $(1, n)$ (with $n \geq 1$) as a function of the coefficient of restitution. He adopted the model, the analysis, and the response classification of Spanos and Koh [17].

Makris and Konstantinidis [20] compared responses of the rocking block and the linear, viscously damped oscillator to the free and force vibration. The authors highlighted fundamental differences between those two systems and came to the conclusion that rocking structures cannot be represented as an equivalent oscillator and should not be evaluated using response spectra, as proposed by Priestley et al. [16]. Further, Makris and Konstantinidis recommended the rocking spectra as an additional measure of earthquake intensity.

In 2011 ElGawady et al. [21] examined the effect of various materials at the interface of the rocking block and the foundation on the coefficient of restitution. In their study they presented highly improved correspondence between the experimental tests and the analytical model using an arbitrary value of the coefficient of restitution.

In recent years Kalliontzis et al. proposed in their work a modified equation for the coefficient of restitution under assumption of a finite contact length at impact rather than point impact. They also showed the improved agreement between the experimental results and the classical model with a modified value of the coefficient of restitution. However the authors could not precisely determine the contact length at impact.

As for the multi block system, the work of Psycharis [6] was the first detailed analysis of the response of the dual-body system, in which one rectangular block is placed on top of another. The author categorized all possible rocking patterns depending on the relative position of the blocks, under the assumption that the friction is large enough to prevent sliding. Furthermore, he derived the governing equations of motion and evaluated the rate of energy dissipation for each pattern.

Spanos et al. [17] further applied numerical integration for the two-body system of [23] and concluded that both implementation and solution are time intensive. Kounadis [25] came to a similar conclusion and recommended investigation of numerical methods.

To the authors best knowledge, few experiments were done on dual- and multi-block system, thus there is a limited experimental data base. The experimental study is very important for validation of the numerical solutions and for the possibility of predicting the behavior of such structures. For these reasons, the experimental study, described in this thesis, was conducted.

Chapter 2

Theory

2.1 Dynamic analysis of single rigid block

A study by Housner [7] has provided the basic understanding on the rocking response of a rigid body. Following his work, let us consider the two-dimensional problem of a symmetric rigid block resting on a rigid horizontal foundation, as shown in Figure 2.1. It provides a reasonable representation of a block-like structures that rock about two parallel edges of their bases. To simulate ground motion, an arbitrary displacement in horizontal and vertical direction can be given to the foundation in the model. Herein, for simplicity, only horizontal excitation will be considered. Furthermore, the coefficient of friction between the block and the foundation is assumed to be sufficiently large so that sliding is prevented. In that case, the block either moves rigidly with the ground, when the excitation is small, or it is set into rocking; in latter case it will oscillate about one of its edges. It is assumed that the block and foundation surfaces,which are in contact, are perfectly smooth so that the block will rock only around corner edges O and O' and not around any intermediate points. For rocking response, the rigid block is characterized by its mass, m, its mass moment of inertia about corner edge O or O', I_o, and the location of the mass center, defined with the distance from either base corner, $R = \sqrt{b^2 + h^2}$ and the angle between R and the vertical when the body is at rest, $\theta_c = \cot^{-1}(h/b)$ (Figure 2.1). Here θ_c is also the critical or maximum angle to which the block can be ed without toppling under gravity alone. The rotation of the block from vertical position is measured by the angle $\theta(t)$. A positive $\theta(t)$ indicates that the block is rotating around the corner O, and a negative indicates rotation about corner O'.

When subjected to horizontal base acceleration $\ddot{x}_g$, the block will be set into rocking when the overturning moment of the horizontal inertia force about one corner exceeds the restoring moment due to the weight of the block:

$$\begin{gathered} m\ddot{x}_g h > mgb \\ \text{or} \\ \ddot{x}_g > (\frac{b}{h})g \end{gathered} \tag{2.1}$$

where g denotes acceleration of the gravity.

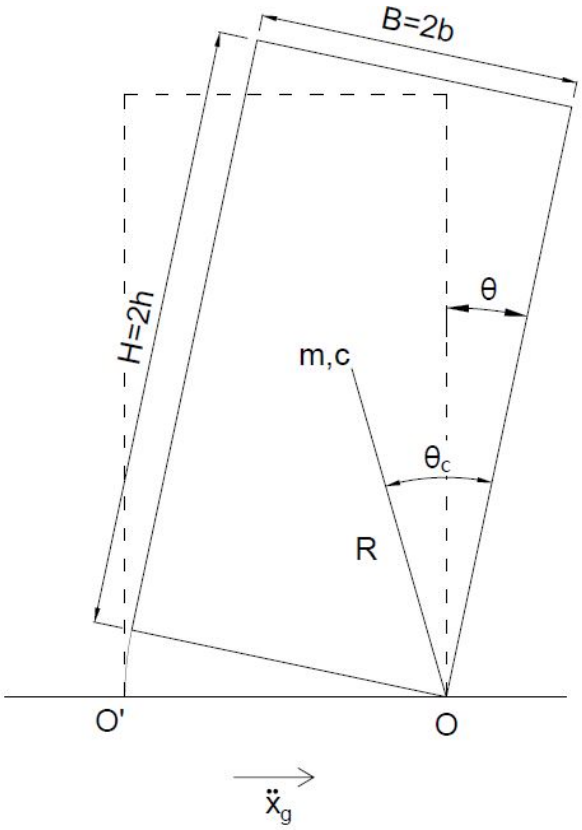

Fig. 2.1: Rigid block geometry

2.1.1 Equation of motion

When the block rotates about corner O or O', the equations of motion of block, governing angle θ from the vertical (Figure 2.1) are derived by considering the equilibrium of moments about the centers of rotation O and O', respectively

$$I_o\ddot{\theta} + mgR\sin(\theta_c - \theta) = -mR\cos(\theta_c - \theta)\ddot{x}_g \tag{2.2}$$

and

$$I_o\ddot{\theta} - mgR\sin(\theta_c + \theta) = -mR\cos(\theta_c + \theta)\ddot{x}_g. \tag{2.3}$$

These two equations combined give one equation of motion, namely

$$I_o\ddot{\theta} + mgR\sin(\theta_c - |\theta|)S_\theta = -mR\cos(\theta_c - |\theta|)\ddot{x}_g \tag{2.4}$$

where S_θ is a signum function defined by

$$S_\theta = \begin{cases} 1 & \theta > 0 \\ -1 & \theta < 0 \end{cases}. \tag{2.5}$$

Equation 2.4 is non-linear in two respects. First, the trigonometric functions of θ features a mild non-linearity; though in most cases these can be linearized (e.g. [7] or [17]). The second source of non-linearity is the change in equation every time the block changes the center of rotation, alternating between O and O' (i.e. after each impact of the block on the foundation). Expanding the trigonometric terms in equation 2.4 leads to

$$I_o\ddot{\theta} + mgR(\sin\theta_c\cos|\theta| - \cos\theta_c\sin|\theta|)S_\theta = -mR(\cos\theta_c\cos|\theta| + \sin\theta_c\sin|\theta|)\ddot{x}_g. \tag{2.6}$$

Further, for small angels of rotation, one can write $\sin\theta \cong \theta$ and $\cos\theta \cong 1$. That leads to the form

$$I_o\ddot{\theta} + mgR(\sin\theta_c - \cos\theta_c|\theta|)S_\theta = -mR(\cos\theta_c + \sin\theta_c|\theta|)\ddot{x}_g. \tag{2.7}$$

Assumption $|\theta| \ll H/B$ implies $\sin\theta_c|\theta| \ll \cos\theta_c$, which reducees equation 2.7 to

$$\begin{aligned} &I_o\ddot{\theta} + mgR(\sin\theta_c - \cos\theta_c|\theta|)S_\theta = -mR\cos\theta_c\ddot{x}_g \\ &\text{or} \qquad\qquad . \\ &I_o\ddot{\theta} - mgR\cos\theta_c\theta = -mR\cos\theta_c\ddot{x}_g - mgRS_\theta\sin\theta_c \end{aligned} \tag{2.8}$$

For slender blocks ($H/B > 3$) ([26]) above written equation can be further linearized. Namely, for θ_c being small, $\sin\theta_c = \theta_c$ and $\cos\theta_c = 1$, the equation 2.8 can then be written as

$$I_o\ddot{\theta} + mgRS_\theta(\theta_c - |\theta|) = -mR\ddot{x}_g. \tag{2.9}$$

Equations 2.8 and 2.9 are valid as long as $\theta \neq 0$. When $\theta = 0$ an impact occurs between the block and the foundation. Depending on the assumptions of the system and impact model the post impact response can be pure rocking, or some of the other response modes [4]. In this thesis only pure rocking is considered, by assuming that the static friction coefficient is large enough to prevent any sliding displacement of the contact point, and that the impact is inelastic, i.e. there is no bouncing. Under these assumptions the rotation continues smoothly about the point O' and the angular momentum is conserved. Equating the angular momentum about O' immediately before the impact to that immediately after the impact gives

$$I_o\dot{\theta}_1 - 2mRb\sin\theta_c\dot{\theta}_1 = I_o\dot{\theta}_2 \tag{2.10}$$

where $\dot{\theta}_1$ and $\dot{\theta}_2$ are the angular velocities before and after the impact, respectively. Just before and just after the impact, angle of rotation θ is zero and therefore the potential energy stored in the system is equal to zero. At these two moments the total energy of the system is in the form of the kinetic energy. The ratio of the kinetic energies is

$$r = \frac{\frac{1}{2}I_o\dot{\theta}_2^2}{\frac{1}{2}I_o\dot{\theta}_1^2} = \left(\frac{\dot{\theta}_2}{\dot{\theta}_1}\right)^2 \tag{2.11}$$

and the energy loss due to impact is equal to $1 - r$. Using equation 2.10, r can be expressed as

$$r = \left[1 - \frac{2mR^2}{I_o} \sin^2 \theta_c\right]^2 . \tag{2.12}$$

Following the concept of classical analytical dynamics, the coefficient of restitution is defined as

$$e = \frac{\dot{\theta}_2}{\dot{\theta}_1} \tag{2.13}$$

which combined with equation 2.10, and noting that for a rectangular block $I_o = \frac{4}{3}mR^2$,yields

$$e = 1 - \frac{3}{2} \sin^2 \theta_c \tag{2.14}$$

.

Thus, the energy loss due to impact is $1 - e^2$. The higher the coefficient of restitution, the smaller is the energy loss due to an impact.

As it can be seen from equation 2.14 the coefficient of restitution depends only on the block slenderness ratio H/B or θ_c. It is independent both form the size of the block and the angular velocity before the impact. The values are exactly valid only for the idealized conditions of the rigid block and the foundation. Based on experimental evidence it is just approximately valid for real conditions. Priestley et al. [16] stated in their work "The value of $e = 0.87$ was adopted to provide a best fit with the experimental data, and is substantially different from the value $e = 0.70$ [based on conservation of angular momentum]". Same dissimilarity is noted by Aslam et al. [14], who tested concrete blocks with slightly concave bases in series of free rocking experiments. The equations of motion are also numerically integrated, reducing the angular velocity by the ratio e after every impact. They had to adjust e to get a good match between numerical and experimental results. The coefficient of restitution depends besides the slenderness ratio, also on materials of the block and the foundation [21], which explains mentioned dissimilarity between coefficient of restitution based on conservation of momentum under idealized conditions, i.e. equation 2.14, and the experimental values.

2.1.2 Free rocking

When the block is rotated about O through an angle θ_0 and released with initial displacement, it will be set into rocking about O and O'. The resulting free vibration of slender block is governed by equation 2.9 with base acceleration set to zero:

$$\begin{aligned} &I_o\ddot{\theta} + mgR(\theta_c - |\theta|) = 0 \\ &\text{or} \\ &\ddot{\theta} - p^2\theta = -p^2\theta_c \end{aligned} \tag{2.15}$$

where

$$p^2 = \sqrt{\frac{mgR}{I_0}} \tag{2.16}$$

is the natural frequency of small oscillations, under gravity of the block suspended from one of its corners. For a rectangular block it yields

$$p = \sqrt{\frac{3g}{4R}}. \tag{2.17}$$

The general solution of equation 2.15 is given by

$$\theta(t) = C_1 \cosh pt + C_2 \sinh pt + \theta_c. \tag{2.18}$$

Equation 2.18 subjected to initial conditions $\theta = \theta_0$ and $\dot{\theta} = 0$ at $t = 0$ yields

$$\theta(t) = \theta_c - (\theta_c - \theta_0) \cosh pt \tag{2.19}$$

which is valid for $0 \leq t \leq t_1$ in which t_1 denotes the time to the first impact. In other words equation 2.19 describes the rotation of the block about the point O as it falls back into the vertical position after it is released from the rest with initial displacement θ_0. After the impact, the block will rotate about O' and if there is no energy loss during the impact it will rotate through an angle $\theta = -\theta_0$. At this instant one complete cycle of vibration has been completed. Time T required to complete this cycle is the period of free vibration. It will be equal to the time t_1, determined from equation 2.19, multiplied by four:

$$T = 4t_1 = \frac{4}{p} \cosh^{-1}(\frac{1}{1 - \theta_0/\theta_c}). \tag{2.20}$$

2.2 Dynamic analysis of two rigid block assemblies

Opposed to the case of a single rocking block, dynamic behavior of assemblies of blocks has not been studied enough, because of complexity of the problem. Its complexity is associated with a continues transition from one pattern of motion to another, each being governed by a different set of highly non-linear equations.

In this section the simplest case of assemblies of blocks, i.e. two-block assemblies, in which one block is symmetrically placed over the other, is examined. This configuration can be thought as a model of a structure consisting of two pieces, one a top of other, free to rock, e.g. a statue, piece of machinery or any other object placed on a block-like base. All possible configuration patterns exhibited by the two rigid block (2-DOF) assemblies during rocking motion are classified and criteria for initiation of motion are determined. Further for each pattern the corresponding equations of motion are derived and transition criteria between patterns are formulated.

Two rigid block assemblies studied here is depicted in Figure 2.2. It consists of two symmetric rigid blocks. The upper block, which in the following will be called block 2, lies symmetrically

on the top of the lower one, which will be called block 1, and the latter rests on a horizontal rigid foundation. The blocks have masses m_i, and centroid moments of inertia I_{Ci}, where i is the block index. The center of masses for each block is denoted by C_i, and its location is defined with the distance from the base corner R_i and the angle between, R_i, and the vertical of the block, θ_{Ci}. Assuming that the friction between two blocks and between block 1 and the foundation, is large enough to prevent sliding, the system posses two degrees of freedom, namely, θ_1 and θ_2, denoting respectively the angles of rotation of block 1 and block 2 from the vertical position.

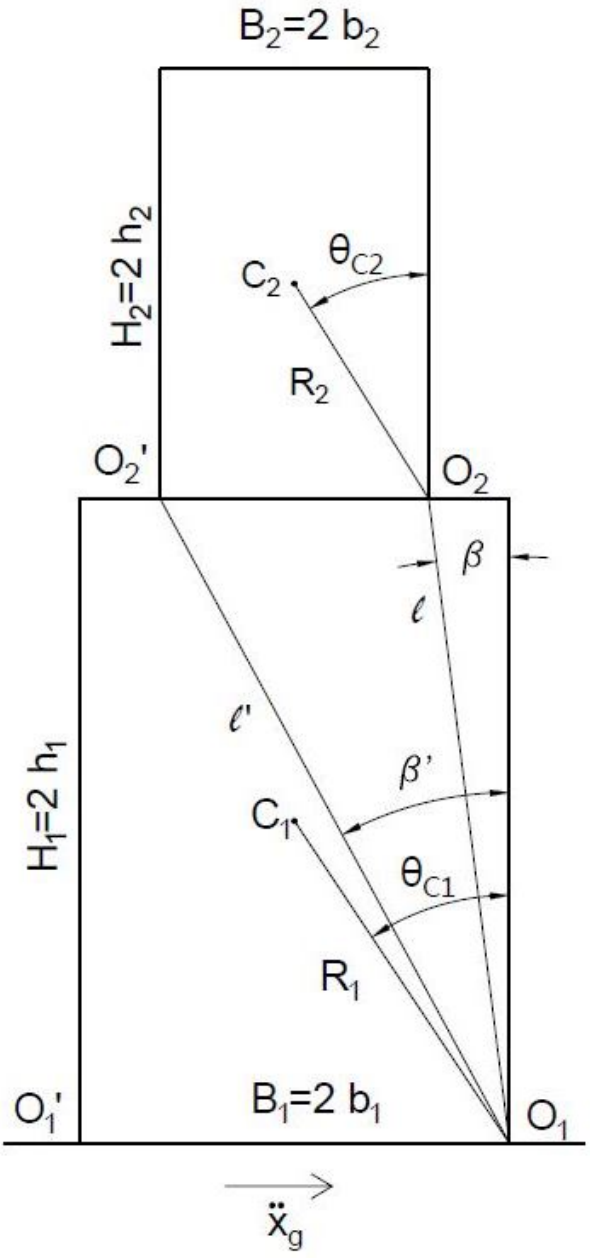

Fig. 2.2: Geometric model of two block assemblies

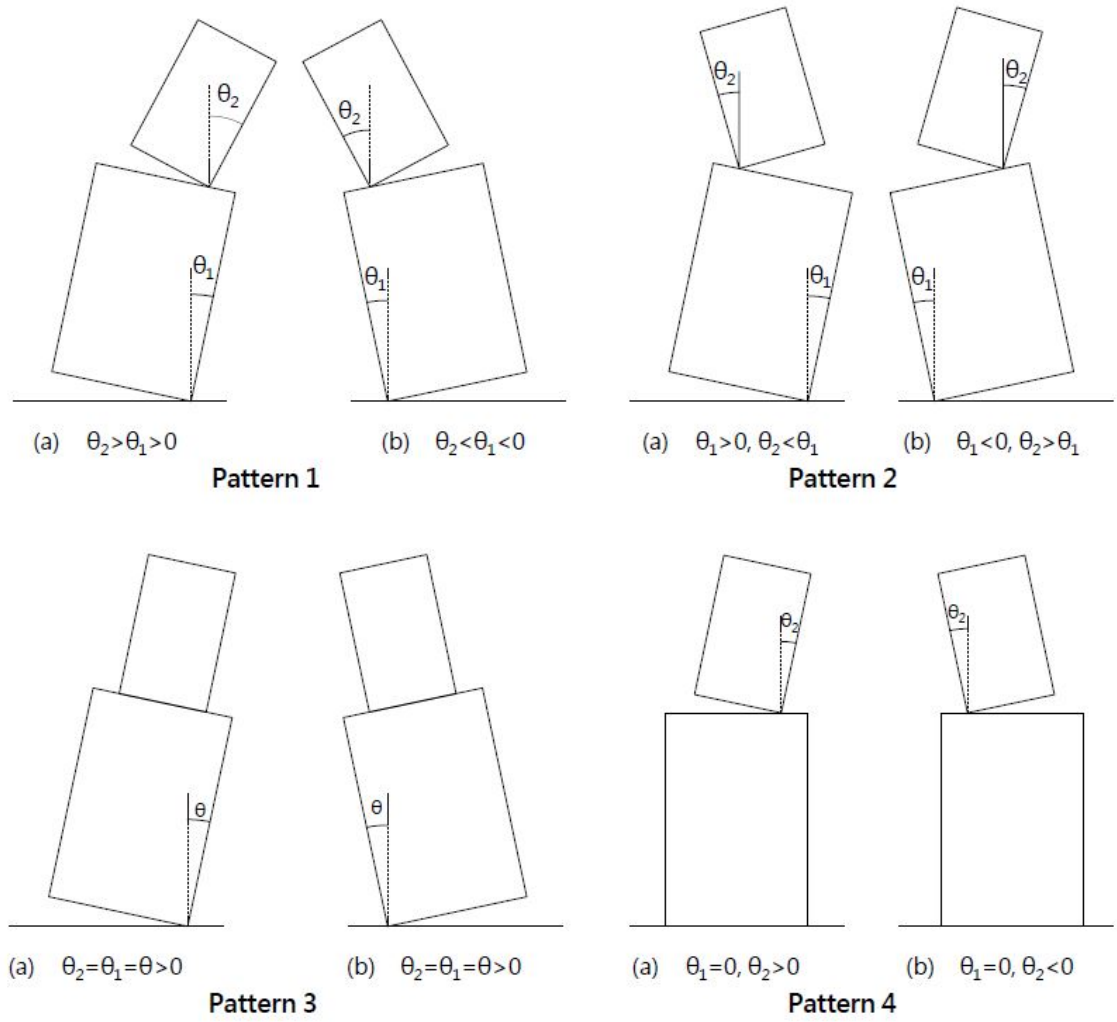

Fig. 2.3: Patterns of rocking motion for the system

Tab. 2.1: Equations governing transition between patterns

to / from		Pattern 1		Pattern 2		Pattern 3		Pattern 4	
		a	b	a	b	a	b	a	b
rest		-	-	-	-	2.21	2.23	2.24	2.25
Pattern 1	a	-	-	2.78	2.76	2.79	-	-	-
	b	-	-	2.76	2.78	-	2.79	-	-
Pattern 2	a	2.81	??	-	-	2.82	-	-	-
	b	??	2.81	-	-	-	2.82	-	-
Pattern 3	a	2.66	2.83	2.69	-	-	2.84	-	-
	b	2.83	2.70	-	2.71	2.84	-	-	-
Pattern 3	a	2.72	2.85	-	2.73	-	-	-	2.86
	b	2.85	2.74	2.75	-	-	-	2.86	-

Subjected to the base excitation, here for simplicity, only excitation in horizontal direction, $\ddot{x}_g$, is considered, the system may exhibit the four possible patterns of rocking motion classified in Figure 2.3 with respect to the angels of rotation θ_1 and θ_2. First two patterns involve 2-DOF system response, and they are discretized depending whether the two blocks rotate in the same or opposite direction. Patterns 3 and 4 reflect SDOF system response. In particular, pattern 3 describes the motion of the system rocking as one rigid structure ($\theta_1 = \theta_2$), and pattern 4 concerns the case where only the top block experience rotation ($\theta_1 = 0, \theta_2 \neq 0$). Depending whether the rotation is positive or negative each pattern is divided into subcases (a) and (b). This discretization is necessary because a different set of equations of motion holds in each subcase.

2.2.1 Initiation of motion

When subjected to the horizontal excitation, the system starts rocking when the overturning moment of the horizontal inertia force about one edge exceeds the restoring moment due to the weight(s) of the block(s). This may happen for the whole system, in which case the system starts rocking in pattern 3, or for the block 2 only, which then starts rocking in pattern 4 as can be seen in Figure 2.4. The criteria for initiation of motion are given bellow:

- transition from rest to mode 3a requires

$$-h\ddot{x}_g > b_1 g \tag{2.21}$$

  where

$$h = \frac{m_1 h_1 + m_2(2h_1 + h_2)}{m_1 + m_2} \tag{2.22}$$

  is the distance of the mass center of system from the base of block 1

- transition from rest to mode 3b requires

$$h\ddot{x}_g > b_1 g \tag{2.23}$$

- transition from rest to mode 4a requires

$$-h_2\ddot{x}_g > b_2 g \tag{2.24}$$

- transition from rest to mode 4b requires

$$h_2\ddot{x}_g > b_2 g. \tag{2.25}$$

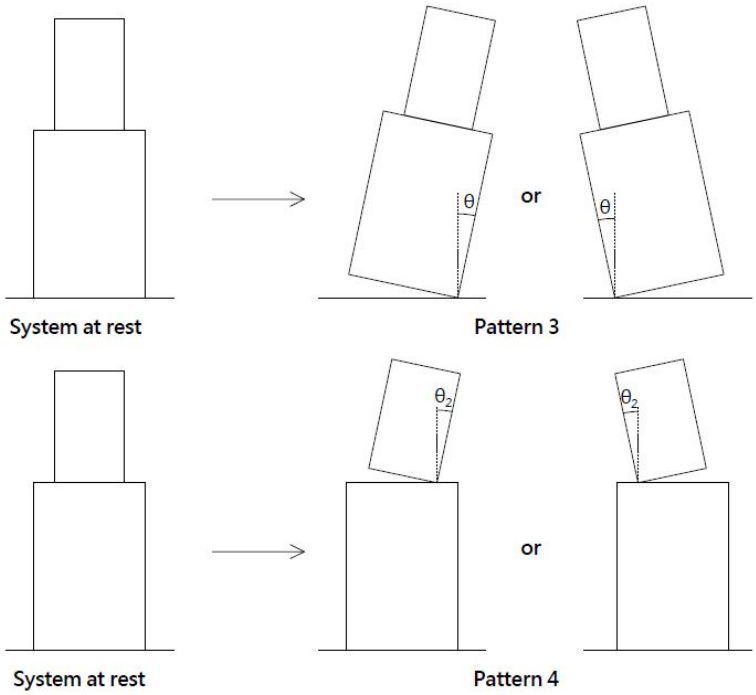

Fig. 2.4: Initiation of motion

2.2.2 Equations of motion

The equations of motion of the system for the possible patterns and their subcases are derived applying Lagrange's method. The Lagrange's equations of motion for 2-DOF system are given in the form

$$\frac{d}{dt}\left(\frac{\partial T}{\partial \dot{\theta}_i}\right) - \frac{\partial T}{\partial \theta_i} + \frac{\partial V}{\partial \theta_i} = 0 \tag{2.26}$$

where

$$T = T_1 + T_2 = \frac{1}{2}\sum_{i=1}^{2}(I_{C_i}\dot{\theta}_i^2 + m_i v_{C_i}^2) \tag{2.27}$$

is the kinetic energy of the system and

$$V = V_1 + V_2 = \sum_{i=1}^{2}(m_i h_{C_i} g) \tag{2.28}$$

is the gravitational potential energy of the system. In the above equations v_{C_i} detonates the velocity of the i-th center of mass, with $v_{C_i}^2 = \dot{x}_{C_i}^2 + \dot{y}_{C_i}^2$, and h_{C_i} the distance of the i-th center of mass from the ground.

2.2.2.1 Equations for pattern 1

In the first pattern both blocks are rotating in the same direction. They would either rotate in positive direction, $\theta_i > 0$, i.e. pattern 1a, or in negative, $\theta_i < 0$, i.e. pattern 1b. First the case where system is rocking in pattern 1a will be considered. Assuming there is no bouncing, and

according to the Figure 2.5a the total horizontal and vertical displacement of the mass center of block 1, respectively, are given by:

$$\begin{aligned} x_{C_1} &= x_g + b_1 - R_1 \sin(\theta_{C_1} - \theta_1) \\ y_{C_1} &= R_1 \cos(\theta_{C_1} - \theta_1) - h_1 \,. \end{aligned} \tag{2.29}$$

Similary the total horizontal and vertical displacement of mass center of block 2 are, respectively (Figure 2.5a)

$$\begin{aligned} x_{C_2} &= x_g + b_2 - R_2 \sin(\theta_{C_2} - \theta_2) + l \sin\beta + l \sin(\theta_1 - \beta) \\ y_{C_2} &= R_2 \cos(\theta_{C_2} - \theta_2) + l \cos(\theta_1 - \beta) - 2h_1 - h_2 \,. \end{aligned} \tag{2.30}$$

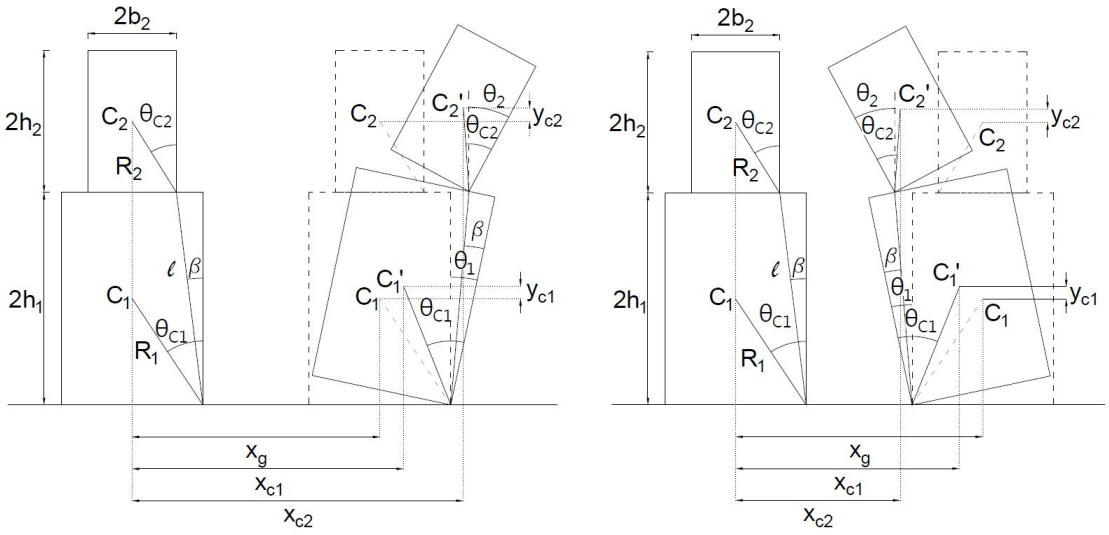

(a) $\theta_2 > \theta_1 > 0$ **(b)** $\theta_2 < \theta_1 < 0$

Fig. 2.5: Pattern 1 displacement under horizontal excitation

Differentiating equations 2.29 and 2.30 with respect to time, gives

$$\begin{aligned} \dot{x}_{C_1} &= \dot{x}_g + R_1\dot{\theta}_1 \cos(\theta_{C_1} - \theta_1) \\ \dot{y}_{C_1} &= R_1\dot{\theta}_1 \sin(\theta_{C_1} - \theta_1) \\ \dot{x}_{C_2} &= \dot{x}_g + R_2\dot{\theta}_2 \cos(\theta_{C_2} - \theta_2) + l\dot{\theta}_1 \cos(\theta_1 - \beta) \\ \dot{y}_{C_2} &= R_2\dot{\theta}_2 \sin(\theta_{C_2} - \theta_2) - l\dot{\theta}_1 \sin(\theta_1 - \beta) \,. \end{aligned} \tag{2.31}$$

The velocities of the mass center of block 1 and block 2 are then derived:

$$\begin{aligned} v_{C_1}^2 &= \dot{x}_{C_1}^2 + \dot{y}_{C_1}^2 \\ &= \dot{x}_g^2 + R_1^2\dot{\theta}_1^2 + 2R_1\dot{\theta}_1\dot{x}_g\cos(\theta_{C_1} - \theta_1) \end{aligned} \tag{2.32}$$

$$\begin{aligned} v_{C_2}^2 &= \dot{x}_{C_2}^2 + \dot{y}_{C_2}^2 \\ &= \dot{x}_g^2 + R_2^2\dot{\theta}_2^2 + l^2\dot{\theta}_1^2 + 2R_2\dot{\theta}_2\dot{x}_g\cos(\theta_{C_2} - \theta_2) + 2l\dot{\theta}_1\dot{x}_g\cos(\theta_1 - \beta)\,. \end{aligned} \tag{2.33}$$

Using equations 2.32 and 2.33 kinetic energy defined in equation 2.27, after suitable mathematical manipulations, is written as

$$\begin{aligned} T = &\frac{1}{2}m_1[R_1^2\dot{\theta}_1^2 + \dot{x}_g^2 + 2R_1\dot{\theta}_1\dot{x}_g\cos(\theta_{C_1} - \theta_1)] + \frac{1}{2}I_{C_1}\dot{\theta}_1^2 + \\ &+ \frac{1}{2}m_2[l^2\dot{\theta}_1^2 + R_2^2\dot{\theta}_2^2 + \dot{x}_g^2 + 2l\dot{\theta}_1\dot{x}_g\cos(\theta_1 - \beta) + \\ &+ 2R_2\dot{\theta}_2\dot{x}_g\cos(\theta_{C_2} - \theta_2) + 2R_2l\dot{\theta}_1\dot{\theta}_2\cos(\theta_1 - \theta_2 + \theta_{C_2} - \beta)] + \frac{1}{2}I_{C_2}\dot{\theta}_2^2\,. \end{aligned} \tag{2.34}$$

The gravitational potential energy according to the equation 2.28 for the pattern 1a is given by:

$$\begin{aligned} V &= m_1gy_{C_1} + m_2gy_{C_2} \\ &= m_1g[R_1\cos(\theta_{C_1} - \theta_1) - h_1] + m_2g[R_2\cos(\theta_{C_2} - \theta_2) + l\cos(\theta_1 - \beta) - 2h_1 - h_2]\,. \end{aligned} \tag{2.35}$$

Using equations 2.34 and 2.35 the necessary derivatives for the use in Lagrange's equation (2.26) are obtained, specifically

$$\frac{\partial T}{\partial\dot{\theta}_1} = (I_{O_1} + m_2l^2)\dot{\theta}_1 + m_2R_2l\cos\gamma_{1a}\dot{\theta}_2 + m_1R_1\dot{x}_g\cos(\theta_{C_1} - \theta_1) + m_2l\dot{x}_g\cos(\theta_1 - \beta)$$

$$\begin{aligned} \frac{d}{dt}\left(\frac{\partial T}{\partial\dot{\theta}_1}\right) = &(I_{O_1} + m_2l^2)\ddot{\theta}_1 + m_2R_2l[\cos(\gamma_{1a})\ddot{\theta}_2 - \sin\gamma_{1a}(\dot{\theta}_1 - \dot{\theta}_2)\dot{\theta}_2] + \\ &+ m_1R_1[\ddot{x}_g\cos(\theta_{C_1} - \theta_1) + \dot{x}_g\sin(\theta_{C_1} - \theta_1)\dot{\theta}_1] + m_2l[\ddot{x}_g\cos(\theta_1 - \beta) - \dot{x}_g\sin(\theta_1 - \beta)\dot{\theta}_1] \end{aligned}$$

$$\frac{\partial T}{\partial\theta_1} = m_1R_1\dot{\theta}_1\dot{x}_g\sin(\theta_{C_1} - \theta_1) - m_2l\dot{\theta}_1\dot{x}_g\sin(\theta_1 - \beta) - m_2R_2l\dot{\theta}_1\dot{\theta}_2\sin\gamma_{1a}$$

$$\frac{\partial V}{\partial\theta_1} = m_1gR_1\sin(\theta_{C_1} - \theta_1) - m_2gl\sin(\theta_1 - \beta)$$

and

$$\begin{aligned}
\frac{\partial T}{\partial \dot{\theta}_2} &= I_{O_2}\dot{\theta}_2 + m_2 R_2 l\cos\gamma_{1a}\dot{\theta}_1 + m_2 R_2 \dot{x}_g \cos(\theta_{C_2} - \theta_2) \\
\frac{d}{dt}\left(\frac{\partial T}{\partial \dot{\theta}_2}\right) &= I_{O_2}\ddot{\theta}_2 + m_2 R_2 l[\cos(\gamma_{1a})\ddot{\theta}_1 - \dot{\theta}_1 \sin\gamma_{1a}(\dot{\theta}_1 - \dot{\theta}_2)] + \\
&\quad + m_2 R_2[\ddot{x}_g \cos(\theta_{C_2} - \theta_2) + \dot{x}_g\dot{\theta}_2 \sin(\theta_{C_2} - \theta_2)] \\
\frac{\partial T}{\partial \theta_2} &= m_2 R_2 \dot{\theta}_2 \dot{x}_g \sin(\theta_{C_2} - \theta_2) + m_2 R_2 l\dot{\theta}_1\dot{\theta}_2 \sin\gamma_{1a} \\
\frac{\partial V}{\partial \theta_2} &= m_2 g R_2 \sin(\theta_{C_2} - \theta_2)\,.
\end{aligned}$$

Where I_{O_1} and I_{O_2} are moments of inertia about the points O_1 and O_2, respectively and γ_{1a} is defined by

$$\gamma_{1a} = \theta_{C_2} - \beta + \theta_1 - \theta_2\,. \tag{2.36}$$

The equations of motion for rocking response in pattern 1a are obtained from equation 2.26 and written in the form

$$\begin{aligned}
&(I_{O_1} + m_2 l^2)\ddot{\theta}_1 + m_2 R_2 l\cos\gamma_{1a}\ddot{\theta}_2 + m_2 R_2 l\sin\gamma_{1a}\dot{\theta}_2^2 + m_1 g R_1 \sin(\theta_{C_1} - \theta_1) \\
&+ m_2 g l\sin(\beta - \theta_1) = -[m_1 R_1 \cos(\theta_{C_1} - \theta_1) + m_2 l\cos(\beta - \theta_1)]\ddot{x}_g \\
&\text{and} \\
&I_{O_2}\ddot{\theta}_2 + m_2 R_2 l\cos\gamma_{1a}\ddot{\theta}_1 - m_2 R_2 l\sin\gamma_{1a}\dot{\theta}_1^2 + m_2 g R_2 \sin(\theta_{C_2} - \theta_2) \\
&= -m_2 R_2 \cos(\theta_{C_2} - \theta_2)\ddot{x}_g
\end{aligned} \tag{2.37}$$

which are valid for $\theta_2 > \theta_1 > 0$.

For pattern 1b, the total horizontal and vertical displacement of the mass center of block 1 and block 2 are, respecivaly

$$\begin{aligned}
x_{C_1} &= x_g - b_1 + R_1 \sin(\theta_{C_1} + \theta_1) \\
y_{C_1} &= R_1 \cos(\theta_{C_1} + \theta_1) - h_1
\end{aligned} \tag{2.38}$$

and

$$\begin{aligned}
x_{C_2} &= x_g - b_2 + R_2 \sin(\theta_{C_2} + \theta_2) - l\sin\beta + l\sin(\theta_1 + \beta) \\
y_{C_2} &= R_2 \cos(\theta_{C_2} - \theta_2) + l\cos(\theta_1 + \beta) - 2h_1 - h_2\,.
\end{aligned} \tag{2.39}$$

The governing equations of motion for rocking response in pattern 1b are then similarly derived as for rocking in pattern 1a, and can be expressed in the form

$$
\begin{aligned}
&(I_{O_1} + m_2 l^2)\ddot{\theta}_1 + m_2 R_2 l \cos\gamma_{1b}\ddot{\theta}_2 - m_2 R_2 l \sin\gamma_{1b}\dot{\theta}_2^2 - m_1 g R_1 \sin(\theta_{C_1} + \theta_1) \\
&- m_2 g l \sin(\beta + \theta_1) = -[m_1 R_1 \cos(\theta_{C_1} + \theta_1) + m_2 l \cos(\beta + \theta_1)]\ddot{x}_g \\
&\text{and} \\
&I_{O_2}\ddot{\theta}_2 + m_2 R_2 l \cos\gamma_{1b}\ddot{\theta}_1 + m_2 R_2 l \sin\gamma_{1b}\dot{\theta}_1^2 - m_2 g R_2 \sin(\theta_{C_2} + \theta_2) \\
&= -m_2 R_2 \ddot{x}_g \cos(\theta_{C_2} + \theta_2)
\end{aligned}
\tag{2.40}
$$

which are valid for $\theta_2 < \theta_1 < 0$, and γ_{1b} is defined by

$$
\gamma_{1b} = \theta_{C_2} - \beta - \theta_1 + \theta_2 \,. \tag{2.41}
$$

Using signum function in θ_1, S_{θ_1}, defined as

$$
S_{\theta_1} = \begin{cases} 1 & \theta_1 > 0 \\ -1 & \theta_1 < 0 \end{cases} . \tag{2.42}
$$

Equations 2.37 and 2.40 can be combined, which leads to a compact set of equations for pattern 1, namely,

$$
\begin{aligned}
&(I_{O_1} + m_2 l^2)\ddot{\theta}_1 + m_2 R_2 l \cos\gamma_1\ddot{\theta}_2 + S_{\theta_1} m_2 R_2 l \sin\gamma_1\dot{\theta}_2^2 + S_{\theta_1} m_1 g R_1 \sin(\theta_{C_1} - S_{\theta_1}\theta_1) \\
&+ S_{\theta_1} m_2 g l \sin(\beta - S_{\theta_1}\theta_1) = -[m_1 R_1 \cos(\theta_{C_1} - S_{\theta_1}\theta_1) + m_2 l \cos(\beta - S_{\theta_1}\theta_1)]\ddot{x}_g \\
&\text{and} \\
&I_{O_2}\ddot{\theta}_2 + m_2 R_2 l \cos\gamma_1\ddot{\theta}_1 - S_{\theta_1} m_2 R_2 l \sin\gamma_1\dot{\theta}_1^2 + S_{\theta_1} m_2 g R_2 \sin(\theta_{C_2} - S_{\theta_1}\theta_2) \\
&= -m_2 R_2 \ddot{x}_g \cos(\theta_{C_2} - S_{\theta_1}\theta_2)
\end{aligned}
\tag{2.43}
$$

where γ_1 is given by

$$
\gamma_1 = \theta_{C_2} - \beta + S_{\theta_1}(\theta_1 - \theta_2) \,. \tag{2.44}
$$

2.2.2.2 Equations for pattern 2

In the second pattern, the two blocks are rotating in opposite directions. Pattern 2a describes the response for $\theta_1 > 0$ and pattern 2b for $\theta_1 < 0$, as shown in Figure 2.6a and 2.6b, respectively. The total displacement of block 1 is the same as that of pattern 1a given by equation 2.29. On the other hand the total horizontal and vertical displacement of the mass center of block 2 are given, respectively, by

$$
\begin{aligned}
x_{C_2} &= x_g - b_2 + R_2 \sin(\theta_{C_2} + \theta_2) + l' \sin\beta' - l' \sin(\beta' - \theta_1) \\
y_{C_2} &= R_2 \cos(\theta_{C_2} + \theta_2) + l' \cos(\beta' - \theta_1) - 2h_1 - h_2 \,.
\end{aligned}
\tag{2.45}
$$

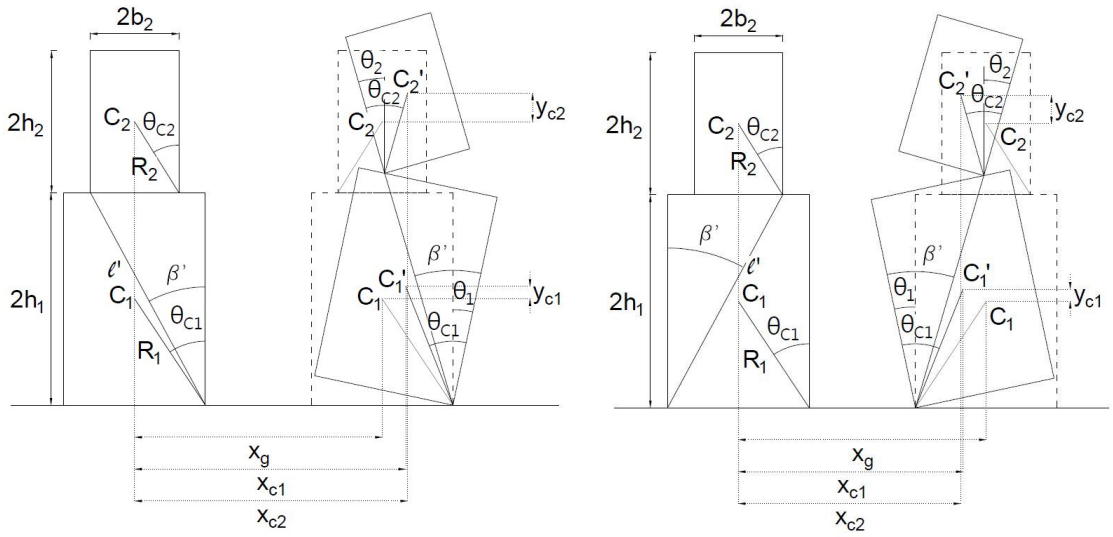

(a) $\theta_1 > 0, \theta_2 < \theta_1$ **(b)** $\theta_1 < 0, \theta_2 > \theta_1$

Fig. 2.6: Pattern 2 displacement under horizontal excitation

The equations of motion for rocking response in pattern 2a are similarly obtained as for rocking in pattern 1a, and can be written in the form

$$\begin{aligned}
&(I_{O_1} + m_2 l'^2)\ddot{\theta}_1 + m_2 R_2 l' \cos\gamma_{2a}\ddot{\theta}_2 - m_2 R_2 l' \sin\gamma_{2a}\dot{\theta}_2^2 + m_1 g R_1 \sin(\theta_{C_1} - \theta_1) \\
&+ m_2 g l' \sin(\beta' - \theta_1) = -[m_1 R_1 \cos(\theta_{C_1} - \theta_1) + m_2 l' \cos(\beta' - \theta_1)]\ddot{x}_g \\
&\text{and} \\
&I_{O_2}\ddot{\theta}_2 + m_2 R_2 l' \cos\gamma_{2a}\ddot{\theta}_1 + m_2 R_2 l' \sin\gamma_{2a}\dot{\theta}_1^2 + m_2 g R_2 \sin(\theta_{C_2} + \theta_2) \\
&= -m_2 R_2 \ddot{x}_g \cos(\theta_{C_2} + \theta_2)
\end{aligned} \tag{2.46}$$

which are valid for $\theta_1 > 0$, and γ_{2b} is defined by

$$\gamma_{2b} = \theta_{C_2} + \beta' - \theta_1 + \theta_2 \,. \tag{2.47}$$

Taking into consideration, that for rocking response in pattern 2b, the angular velocity of the block 1 is negative, the total horizontal and vertical displacement as well as equations of motion are derived in same manner as in the previous patterns. The total horizontal and vertical displacement of block 1 are the same as that of a pattern 1b given by equation 2.38. And for the block 2 are given by

$$\begin{aligned}
x_{C_2} &= x_g + b_2 - R_2 \sin(\theta_{C_2} - \theta_2) - l' \sin\beta' + l' \sin(\beta' + \theta_1) \\
y_{C_2} &= R_2 \cos(\theta_{C_2} - \theta_2) + l' \cos(\beta' + \theta_1) - 2h_1 - h_2 \,.
\end{aligned} \tag{2.48}$$

The equations of motions for pattern 2b are then

$$\begin{aligned}&(I_{O_1} + m_2 l'^2)\ddot{\theta}_1 + m_2 R_2 l' \cos\gamma_{2b}\ddot{\theta}_2 + m_2 R_2 l' \sin\gamma_{2b}\dot{\theta}_2^2 - m_1 g R_1 \sin(\theta_{C_1} + \theta_1) \\ &- m_2 g l' \sin(\beta' + \theta_1) = -[m_1 R_1 \cos(\theta_{C_1} + \theta_1) + m_2 l' \cos(\beta' + \theta_1)]\ddot{x}_g \\ \text{and} \\ &I_{O_2}\ddot{\theta}_2 + m_2 R_2 l' \cos\gamma_{2b}\ddot{\theta}_1 - m_2 R_2 l' \sin\gamma_{2b}\dot{\theta}_1^2 + m_2 g R_2 \sin(\theta_{C_2} - \theta_2) \\ &= -m_2 R_2 \ddot{x}_g \cos(\theta_{C_2} - \theta_2)\end{aligned} \tag{2.49}$$

where

$$\gamma_{2b} = \theta_{C_2} + \beta' + \theta_1 - \theta_2\,. \tag{2.50}$$

Equations 2.46 and 2.49 can be combined to yield compact set of equations for pattern 2:

$$\begin{aligned}&(I_{O_1} + m_2 l'^2)\ddot{\theta}_1 + m_2 R_2 l' \cos\gamma_{2a}\ddot{\theta}_2 - S_{\theta_1} m_2 R_2 l' \sin\gamma_2\dot{\theta}_2^2 + S_{\theta_1} m_1 g R_1 \sin(\theta_{C_1} - S_{\theta_1}\theta_1) \\ &+ S_{\theta_1} m_2 g l' \sin(\beta' - S_{\theta_1}\theta_1) = -[m_1 R_1 \cos(\theta_{C_1} - S_{\theta_1}\theta_1) + m_2 l' \cos(\beta' - S_{\theta_1}\theta_1)]\ddot{x}_g \\ \text{and} \\ &I_{O_2}\ddot{\theta}_2 + m_2 R_2 l' \cos\gamma_2\ddot{\theta}_1 + S_{\theta_1} m_2 R_2 l' \sin\gamma_2\dot{\theta}_1^2 - S_{\theta_1} m_2 g R_2 \sin(\theta_{C_2} + S_{\theta_1}\theta_2) \\ &= -m_2 R_2 \ddot{x}_g \cos(\theta_{C_2} + S_{\theta_1}\theta_2)\end{aligned} \tag{2.51}$$

where S_{θ_1} denotes the signum function in θ_1, and

$$\gamma_2 = \theta_{C_2} + \beta' - S_{\theta_1}(\theta_1 - \theta_2)\,. \tag{2.52}$$

2.2.2.3 Equations for pattern 3

In pattern 3, the two rigid blocks remain in contact, that is, the system rotates as a whole becoming a SDOF system for pattern 3a and 3b ($\theta_1 = \theta_2 = \theta$). The equations of motion of the system governing the common angle θ are derived by considering the equilibrium of moments about the centers of rotation O and O', respectively. These equations, are same as equations 2.2 through 2.4, specifically

$$I_o\ddot{\theta} + mgR\sin(\theta_c - \theta) = -mR\ddot{x}_g\cos(\theta_c - \theta) \tag{2.53}$$

which is valid for $\theta > 0$, and

$$I_o\ddot{\theta} - mgR\sin(\theta_c + \theta) = -mR\ddot{x}_g\cos(\theta_c + \theta) \tag{2.54}$$

which is valid for $\theta < 0$.

Combining equations 2.53 and 2.54 yields compact equation pattern 3, namely

$$I_o\ddot{\theta} + S_\theta mgR\sin(\theta_c - S_\theta\theta) = -mR\ddot{x}_g\cos(\theta_c - S_\theta\theta) \tag{2.55}$$

where S_θ is defined as in equation 2.5.

In the above equations m is the total mass of the system (i.e. $m = m_1 + m_2$), R the distance of the center of gravity of the system from any base corner of of the block 1, θ the angle between R and the vertical and I_o the mass moment of inertia with respect to any base corner of the block 1. The distance of the center of gravity of the system from the base of block 1, i.e. R, is defined by the equation 2.22.

2.2.2.4 Equations for pattern 4

Pattern 4 describes rocking of block 2 alone, with block 1 being still ($\theta_1 = 0; \theta_2 \neq 0$). In that case, the two rigid block system behaves also as a SDOF system, with equation of motion being

$$I_{O_2}\ddot{\theta}_2 + m_2 g R_2 \sin(\theta_{C_2} - \theta_2) = -m_2 R_2 \ddot{x}_g \cos(\theta_{C_2} - \theta_2) \tag{2.56}$$

which is valid for $\theta > 0$ (pattern 4a), and

$$I_{O_2}\ddot{\theta}_2 - m_2 g R_2 \sin(\theta_{C_2} + \theta_2) = -m_2 R_2 \ddot{x}_g \cos(\theta_{C_2} + \theta_2) \tag{2.57}$$

which is valid for $\theta < 0$ (pattern 4b).

And the compact equation for pattern 4 is

$$I_{O_2}\ddot{\theta}_2 + S_{\theta_2} m_2 g R_2 \sin(\theta_{C_2} - S_{\theta_2}\theta_2) = -m_2 R_2 \ddot{x}_g \cos(\theta_{C_2} - S_{\theta_2}\theta_2) \tag{2.58}$$

in whicht S_{θ_2} denotes the signum function in θ_2, defined as

$$S_{\theta_2} = \begin{cases} 1 & \theta_2 > 0 \\ -1 & \theta_1 < 2\,. \end{cases} \tag{2.59}$$

.

2.2.2.5 Linearized equations of motion

The governing equations of motions are highly non-linear and not amenable to exact closed form solutions. In order to simplify these equations, small angles of rotation are assumed, so that approximation $\sin\theta_i = \theta$ and $\cos\theta_i = 1$ can be used and the second order terms are neglected. After suitable mathematical manipulations the linearized equations of motion can be written in matrix form as

- Pattern 1

$$\begin{bmatrix} I_{O_1} + m_2 l & m_2(2h_1h_2 + b_2\xi) \\ m_2(2h_1h_2 + b_2\xi & I_{O_2} \end{bmatrix} \begin{pmatrix} \ddot{\theta}_1 \\ \ddot{\theta}_2 \end{pmatrix} + \begin{bmatrix} -(m_1 + 2m_2)h_1 g & 0 \\ 0 & -m_2 h_2 g \end{bmatrix} \begin{pmatrix} \theta_1 \\ \theta_2 \end{pmatrix} = \begin{pmatrix} -S_{\theta_1}(m_1 b_1 + m_2\xi)g - (m_1 + 2m_2)h_1\ddot{x}_g \\ -S_{\theta_1} b_2 g - m_2 h_2 \ddot{x}_g \end{pmatrix} \tag{2.60}$$

where

$$\xi = b_1 - b_2 \tag{2.61}$$

- Pattern 2

$$\begin{bmatrix} I_{O_1} + m_2 l' & m_2(2h_1h_2 - b_2\xi') \\ m_2(2h_1h_2 - b_2\xi' & I_{O_2} \end{bmatrix} \begin{pmatrix} \ddot{\theta}_1 \\ \ddot{\theta}_2 \end{pmatrix} + \begin{bmatrix} -(m_1 + 2m_2)h_1 g & 0 \\ 0 & -m_2 h_2 g \end{bmatrix} \begin{pmatrix} \theta_1 \\ \theta_2 \end{pmatrix} = \begin{pmatrix} -S_{\theta_1}(m_1 b_1 + m_2 \xi')g - (m_1 + 2m_2)h_1 \ddot{x}_g \\ S_{\theta_1} b_2 g - m_2 h_2 \ddot{x}_g \end{pmatrix} \tag{2.62}$$

where

$$\xi' = 2b_1 - \xi \tag{2.63}$$

- Pattern 3

$$\begin{aligned} I_o\ddot{\theta} - mgh\theta_1 &= -S_\theta 1 m b_2 g - mh\ddot{x}_g \\ \theta_2 &= \theta_1 \end{aligned} \tag{2.64}$$

with h is defined in equation 2.22 and $m = m_1 + m_2$

- Pattern 4

$$\begin{aligned} &\theta_1 = 0 \\ &I_{O_2}\ddot{\theta}_2 - m_2 g h_2 \theta_2 = -S_{\theta_2} m_2 b_2 g - m_2 h_2 \ddot{x}_g \,. \end{aligned} \tag{2.65}$$

It should be noted that non-linearity of the system is not only because of non-linear nature of the equations of motion, but also because of the continues transition between patterns, each one being governed by a different set of equations.

2.2.3 Transition between patterns without impact

Once motion of the system is initiated, it continuously switches from one pattern to another. This transition may occur either due to an impact, between the two blocks or between the block 1 and the ground, or due to a sudden change in a ground excitation. Transition due to an impact is discussed in sections 2.2.4. The only cases of transition between patterns that can happen without an impact are from pattern 3 or 4, if the ground acceleration is strong enough. The criteria for this kind of transition are derived considering overturning and restoring moments. For example, the system can change from pattern 4a to pattern 1a if the overturning moment of the block 1 about point O_1 becomes greater than the restoring moment. All criteria for transition between pattern without an impact criteria are listed bellow [24]:

- from pattern 3a to pattern 1a, Figure 2.7

$$-\cos(\theta_{C_2}-\theta_1)\ddot{x}_g > g\sin(\theta_{C_2}-\theta_1)+r\cos(\theta_{C_2}-\theta_1\dot{\theta}_1^2)+\left[r\sin(\theta_{C_2}+\Theta)+\frac{I_{C_2}}{m_2R_2}\right]\ddot{\theta}_1 \quad (2.66)$$

where

$$r=\sqrt{(2h_1+h_2)^2+b_1^2} \quad (2.67)$$

and

$$\Theta=\tan^{-1}\left(\frac{2h_1+h_2}{b_1}\right) \quad (2.68)$$

- from pattern 3a to pattern 2a, Figure 2.8

$$\begin{aligned}\cos(\theta_{C_2}+\theta_1)\ddot{x}_g > g\sin(\theta_{C_2}+\theta_1)+r\cos(2\theta_1+\theta_{C_2}+\Theta)\dot{\theta}_1^2\\ +\left[r\sin(2\theta_1+\theta_{C_2}+\Theta)+\frac{I_{C_2}}{m_2R_2}\right]\ddot{\theta}_1\,.\end{aligned} \quad (2.69)$$

- from pattern 3b to pattern 1b, Figure 2.9

$$\begin{aligned}\cos(\theta_{C_2}+\theta_1)\ddot{x}_g > g\sin(\theta_{C_2}+\theta_1)-r\sin(\theta_{C_2}-\Theta)\dot{\theta}_1^2\\ -\left[r\cos(\theta_{C_2}-\Theta)-\frac{I_{C_2}}{m_2R_2}\right]\ddot{\theta}_1\end{aligned} \quad (2.70)$$

- from pattern 3b to pattern 2b, Figure 2.10

$$\begin{aligned}-\cos(\theta_{C_2}-\theta_1)\ddot{x}_g > g\sin(\theta_{C_2}-\theta_1)-r\sin(\theta_{C_2}+\Theta)\dot{\theta}_1^2\\ +\left[r\cos(\theta_{C_2}+\Theta)-\frac{I_{C_2}}{m_2R_2}\right]\ddot{\theta}_1\end{aligned} \quad (2.71)$$

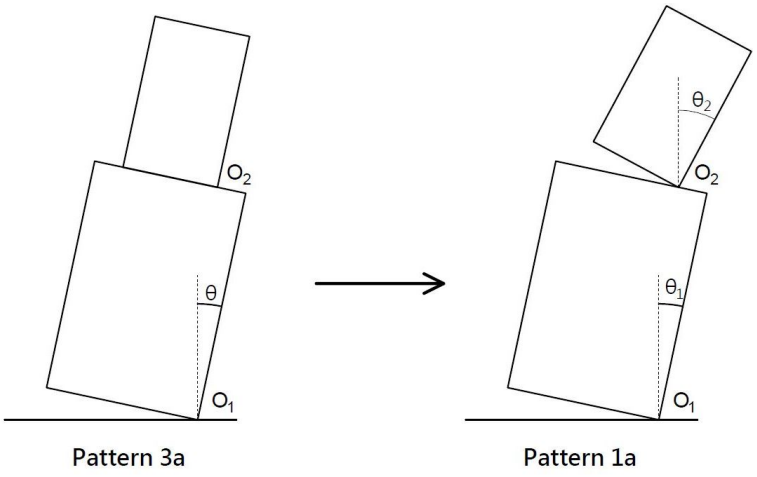

Fig. 2.7: Transition from pattern 3a to pattern 1a

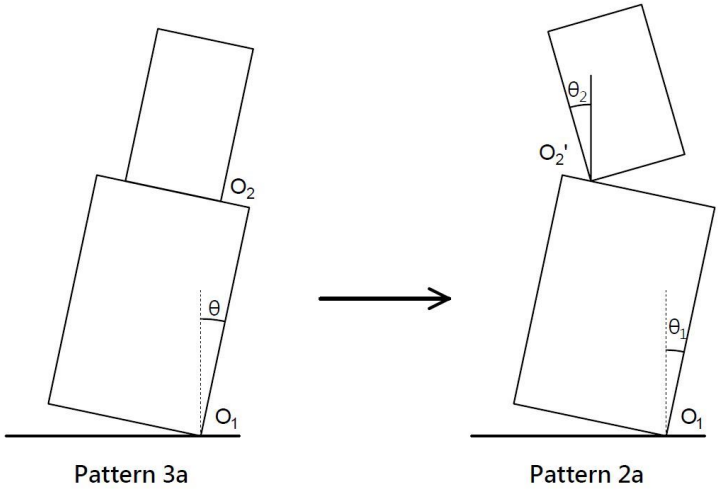

Fig. 2.8: Transition from pattern 3a to pattern 2a

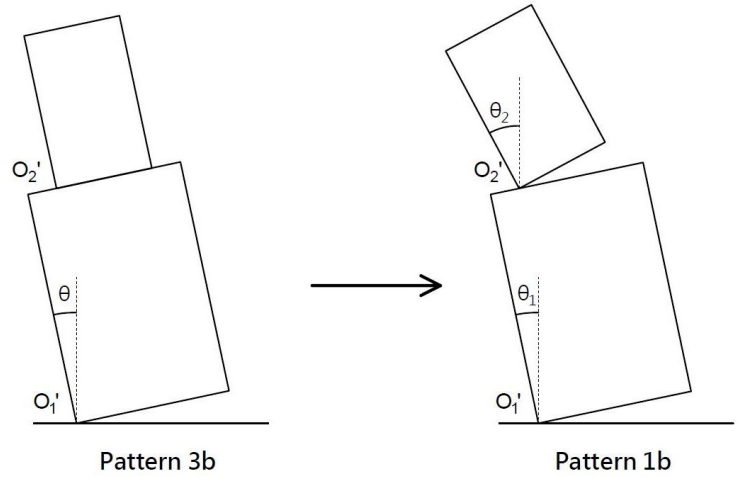

Fig. 2.9: Transition from pattern 3b to pattern 1b

- from pattern 4a to pattern 1a, Figur 2.11

$$\begin{aligned} -(m_1+2m_2)h_1\ddot{x}_g > m_1gb_1 + m_2R_2[2h_1\sin(\theta_{C_2}-\theta_2) - \xi\cos(\theta_{C_2}-\theta_2)]\dot{\theta}_2^2 \\ +m_2R_2[\xi\sin(\theta_{C_2}-\theta_2) + 2h_1\cos\theta_{C_2}-\theta_2]\ddot{\theta}_2 \end{aligned} \tag{2.72}$$

- from pattern 4a to pattern 2b, Figure 2.12

$$\begin{aligned} (m_1+2m_2)h_1\ddot{x}_g > m_1gb_1 - m_2R_2[2h_1\sin(\theta_{C_2}-\theta_2) + \xi'\cos(\theta_{C_2}-\theta_2)]\dot{\theta}_2^2 \\ +m_2R_2[\xi'\sin(\theta_{C_2}-\theta_2) + 2h_1\cos\theta_{C_2}-\theta_2]\ddot{\theta}_2 \end{aligned} \tag{2.73}$$

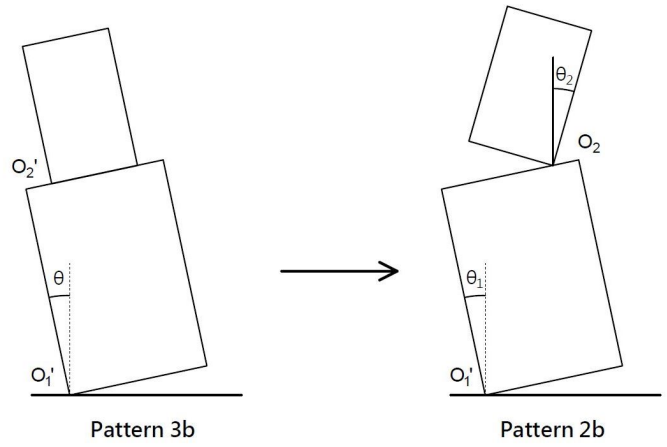

Fig. 2.10: Transition from pattern 3b to pattern 2b

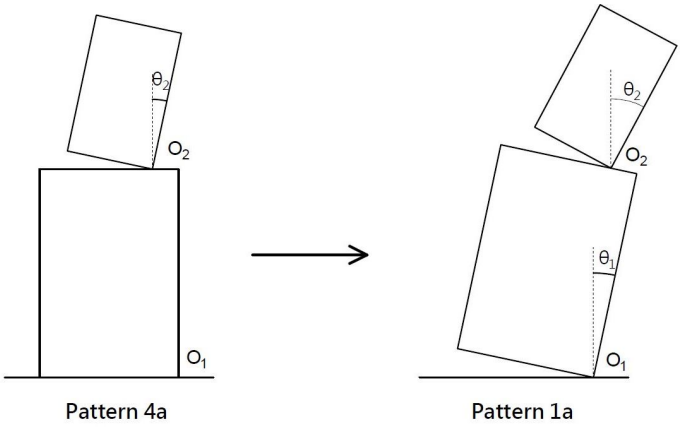

Fig. 2.11: Transition from pattern 4a to pattern 1a

- from pattern 4b to pattern 1b, Figure 2.13

$$\begin{aligned}(m_1+2m_2)h_1\ddot{x}_g > m_1gb_1 + m_2R_2[2h_1\sin(\theta_{C_2}+\theta_2) - \xi\cos(\theta_{C_2}+\theta_2)]\dot{\theta}_2^2 \\ -m_2R_2[\xi\sin(\theta_{C_2}+\theta_2) + 2h_1\cos\theta_{C_2}+\theta_2]\ddot{\theta}_2\end{aligned} \tag{2.74}$$

- from pattern 4b to pattern 2a, Figure 2.14

$$\begin{aligned}-(m_1+2m_2)h_1\ddot{x}_g > m_1gb_1 - m_2R_2[2h_1\sin(\theta_{C_2}+\theta_2) + \xi'\cos(\theta_{C_2}+\theta_2)]\dot{\theta}_2^2 \\ -m_2R_2[\xi'\sin(\theta_{C_2}+\theta_2) - 2h_1\cos\theta_{C_2}+\theta_2]\ddot{\theta}_2\,.\end{aligned} \tag{2.75}$$

In all these cases the initial angular velocities for the new pattern are equal to the corresponding values immediately before transition.

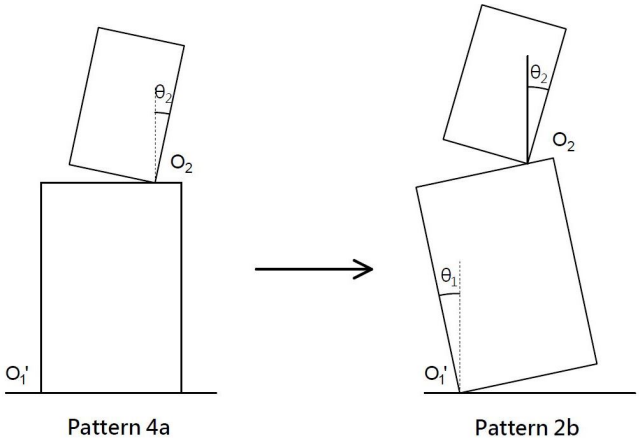

Fig. 2.12: Transition from pattern 4a to pattern 2b

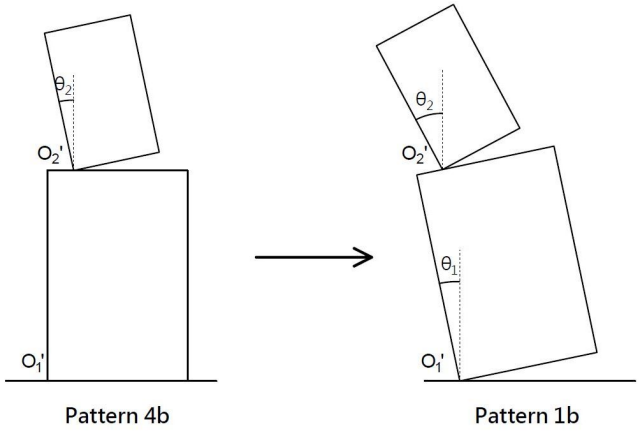

Fig. 2.13: Transition from pattern 4b to pattern 1b

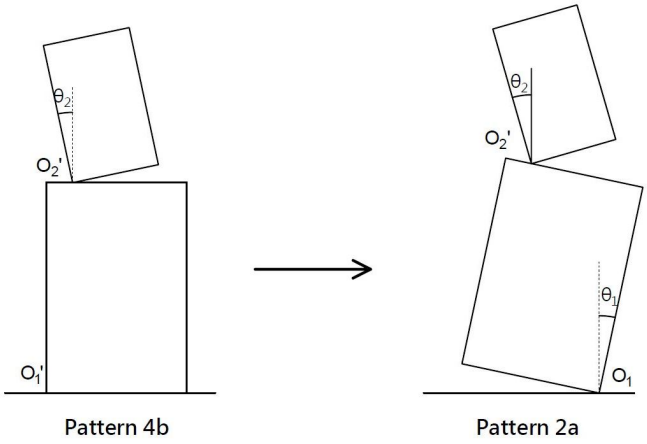

Fig. 2.14: Transition from pattern 4b to pattern 2a

2.2.4 Transition between patterns with impact

1. **Transition from pattern 1a to pattern 2b**
   Let us first assume that the system in rocking in pattern 1a. When the angle of rotation of block 1 becomes zero, the impact occurs which leads to change of rotation pole from O_1 to O_1', i.e. the system switches to pattern 2b (Figure 2.15). It is assumed that the impact takes place only in point O_1' (point impact) and its duration is infinitesimal, implying negligible changes in position and orientation of the blocks. The impact causes instantaneous change in the values of the angular velocities, where the values after the impact, $\dot{\theta}_1^+$ and $\dot{\theta}_2^+$, need to be found. Because all the impact forces pass through the point O_1', the angular momentum of the system about this point is conserved. Further the block 2 is in contact with the block 1 only at point O_2 and therefore all the impact forces, that are transferred to block 2, pass through that point. Thus the angular momentum of block 2 about O_2 is also conserved during impact [23]. Applying this method the system of equations with two unknown, is obtained. $\dot{\theta}_1^+$ and $\dot{\theta}_2^+$ are found by solving the equations. As $\dot{\theta}_1^+$ and $\dot{\theta}_2^+$ denote the angular velocities of blocks 1 and 2, respectively, after impact, let $\dot{\theta}_1^-$ and $\dot{\theta}_2^-$ be the corresponding values before the impact. After some mathematical manipulation, the following equations can be found

$$\begin{aligned} \dot{\theta}_1^+ &= A\dot{\theta}_1^- \\ \dot{\theta}_2^+ &= B\dot{\theta}_1^- + \dot{\theta}_2^- \end{aligned} \tag{2.76}$$

in which

$$A = \frac{C_1C_2 - C_3C_4}{C_5C_1 - C_3C_6}; \quad B = \frac{C_6C_2 - C_5C_4}{C_3C_6 - C_1C_5}$$

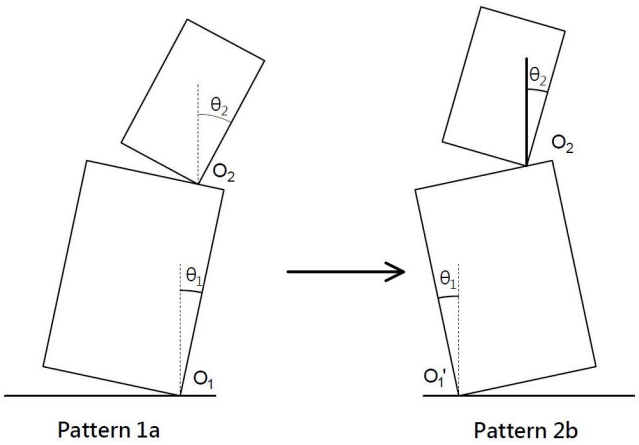

Fig. 2.15: Transition from pattern 1a to pattern 2b

where

$$
\begin{aligned}
C_1 &= I_{O_2} \\
C_2 &= I_{O_1} - 2m_1 b_1^2 + m_2 l[R_2 \cos(\theta_{C_2} - \beta - \theta_2 + 2h_1 \cos\beta - \xi' \sin\beta] \\
C_3 &= I_{O_2} + m_2 R_2[2h_1 \cos(\theta_{C_2} - \theta_2) - \xi' \sin(\theta_{C_2} - \theta_2)] \\
C_4 &= m_2 R_2 l \cos(\theta_{C_2} - \beta - \theta_2) \\
C_5 &= I_{O_1} + m_2 l'[R_2 \cos(\theta_{C_2} + \beta' - \theta_2) + 2h_1 \cos\beta' + \xi' \sin\beta'] \\
C_6 &= m_2 R_2 l' \cos(\theta_{C_2} + \beta' - \theta_2)\,.
\end{aligned}
$$

Note that, from symmetry, above equations also hold for the case of transition from pattern 1b to pattern 2a[24].

2. **Transition from pattern 1a to pattern 2a or to pattern 3a**
As a second case let us again assume that the system is rocking in pattern 1a. However, in this case block 2 impacts block 1, when θ_2 becomes equal to θ_1. A shown in Figure 2.16, after the impact block 2 may either start rocking around O_2' (pattern 2a), or remain in contact with block 1, in which case the system rocks as one rigid body about O_1 (pattern 3a). For pattern 1a is $\theta_2 > \theta_1 > 0$ valid. Thus, in order for transition between pattern 1a and 2a to occur, the relative velocity of block 2 with respect to block 1 must be negative

$$\dot{\theta}_2 - \dot{\theta}_1 < 0\,. \tag{2.77}$$

This means, if block 1 is rotating with a positive angular velocity, impact can occur if block 2 either rotates with negative velocity, or positive bus smaller than the velocity of block 1. In case that block 1 is rotating with a negative angular velocity, block 2 must also rotate with negative, but absolutely greater angular velocity.

In order to determine the angular velocities after an impact, the conservation of the angular momentum about the point O_1 for the whole system and about the point O_2' for block 2, is considered, which yield [24]

$$
\begin{aligned}
\dot{\theta}_1^+ &= A\dot{\theta}_1^- + B\dot{\theta}_2^- \\
\dot{\theta}_2^+ &= C\dot{\theta}_1^- + D\dot{\theta}_2^-
\end{aligned}
\tag{2.78}
$$

where

$$
\begin{aligned}
A &= \frac{E_1E_2 - E_3E_4}{E_5E_1 - E_3E_6}; \quad B = \frac{E_1E_7 - E_3E_8}{E_5E_1 - E_3E_6} \\
C &= \frac{E_6E_2 - E_5E_4}{E_3E_6 - E_1E_5}; \quad D = \frac{E_6E_7 - E_5E_8}{E_3E_6 - E_1E_5}
\end{aligned}
$$

with

$$
\begin{aligned}
E_1 &= I_{O_2} \\
E_2 &= I_{O_1} + m_2 l r \cos(\Theta - \beta) \\
E_3 &= I_{C_2} + m_2 R_2 r \cos(\theta_{C_2} + \Theta - \theta_1 + \theta_2) \\
E_4 &= m_2 R_2 l \cos(\theta_{C_2} + \beta - \theta_1 + \theta_2) \\
E_5 &= I_{O_1} + m_2 l' r \cos(\Theta - \beta') \\
E_6 &= m_2 R_2 l' \cos(\theta_{C_2} + \beta' - \theta_1 + \theta_2) \\
E_7 &= I_{C_2} + m_2 R_2 r \cos(\theta_{C_2} - \Theta + \theta_1 - \theta_2) \\
E_8 &= I_{C_2} + m_2 R_2^2 \cos(2\theta_{C_2}) \,.
\end{aligned}
$$

This was based on assumption that the system switches to pattern 2a. However it is possible that aforementioned equations lead to $\dot{\theta}_2^+ > \dot{\theta}_1^+$, which is physically impossible. In that case block 2 remains in contact with block 1 and the system rocks as one rigid body about O_1 (pattern 3a). The angular velocities of the system can be derived by considering the conservation of the angular momentum about O_1 for the whole system. Namely

$$
\dot{\theta}_1^+ = \dot{\theta}_2^+ = \frac{A_1}{I_o}\dot{\theta}_1^- + \frac{A_2}{I_o}\dot{\theta}_2^- \tag{2.79}
$$

where

$$
\begin{aligned}
A_1 &= I_{O_1} + m_2 l r \cos(\Theta - \beta) \\
A_2 &= I_{C_2} + m_2 R_2 r \cos(\theta_{C_2} - \Theta + \theta_1 - \theta_2) \,.
\end{aligned}
$$

Above equations also hold for the case of transition from pattern 1b to pattern 2b or to pattern 3b [24].

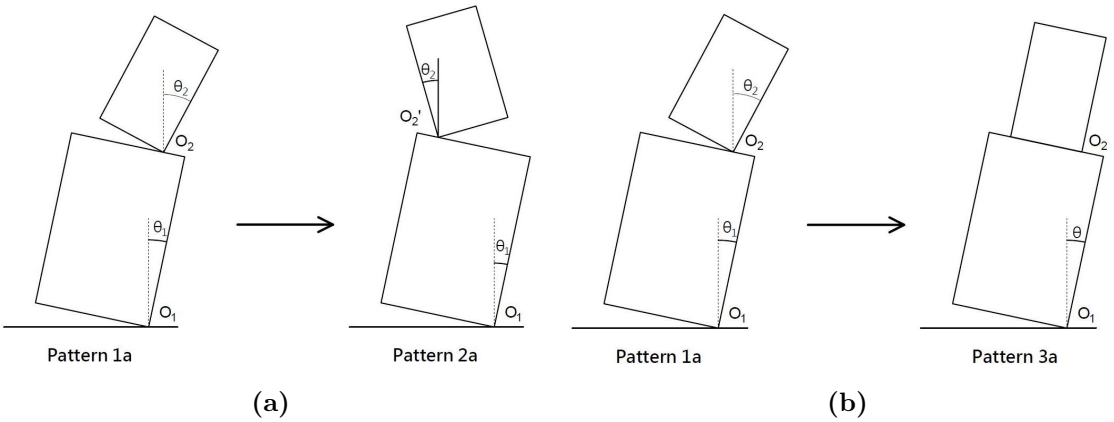

Fig. 2.16: Transition from pattern 1a to pattern 2a or to pattern 3a

3. **Transition from pattern 2a to pattern 1b**
   This case, depicted in Figure 2.17, is similar to case 1. While in first case the blocks were rotating in the same direction before the impact, the blocks in this case have opposite angle of rotation, Pattern 2. Assuming the block 1 is rotating about the point O_1, after the impact the pole of rotation changes to O_1', while the block 2 remains rotating around O_2' (Pattern 1b). By equating the angular momentum, before and after the impact, about the point O_1' for the whole system and about the point O_2' for block 2 the following equations, for the angular velocity after the impact, can be derived

$$\begin{aligned} \dot{\theta}_1^+ &= A\dot{\theta}_1^- + B\dot{\theta}_2^- \\ \dot{\theta}_2^+ &= C\dot{\theta}_1^- + D\dot{\theta}_2^- \end{aligned} \tag{2.80}$$

   where

$$A = \frac{E_1E_2 - E_3E_4}{E_5E_1 - E_3E_6}; \quad B = \frac{E_1E_7 - E_3E_1}{E_5E_1 - E_3E_6}$$
$$C = \frac{E_6E_2 - E_5E_4}{E_3E_6 - E_1E_5}; \quad D = \frac{E_6E_7 - E_5E_1}{E_3E_6 - E_1E_5}$$

   with

$$\begin{aligned} E_1 &= I_{O_2} \\ E_2 &= I_{O_1} - 2m_1b1^2 + m_2l'[R_2\cos(\theta_{C_2} + \beta' + \theta_2) + 2h_1\cos\beta' - \xi\sin\beta'] \\ E_3 &= I_{C_2} + m_2R_2[2h_1\cos(\theta_{C_2} + \theta_2) + \xi\sin(\theta_{C_2} + \theta_2)] \\ E_4 &= m_2R_2l'\cos(\theta_{C_2} + \beta' + \theta_2) \\ E_5 &= I_{O_1} + m_2l[R_2\cos(\theta_{C_2} - \beta' + \theta_2) + 2h_1\cos\beta + \xi\sin\beta] \\ E_6 &= m_2R_2l\cos(\theta_{C_2} - \beta' + \theta_2) \\ E_7 &= I_{C_2} + m_2R_2[2h_1\cos(\theta_{C_2} - \theta_2) - \xi\sin(\theta_{C_2} - \theta_2)]\,. \end{aligned}$$

   The same equations also hold for the case of transition from pattern 2b to pattern 1a [24].

4. **Transition from pattern 2a to pattern 1a or to pattern 3a**
   In this case the system is initially also rocking in pattern 2a, however block 2 impacts block 1, as shown in Figure 2.18. While the block 1 remains rotating about O_1 after the impact, block 2 either changes pole of rotation to O_2' (Pattern 1a) or remains in contact with block 1, in which case the system is rotating as one rigid body about O_1.

   In order for transition from pattern 2a to pattern 1a to happen, the angular velocity of the block two either greater than the one of the block 1, in case $\dot{\theta}_1 > 0$, or just positive in case the block 1 is rotating with a negative angular velocity. Considering the conservation of the angular momentum about the point O_1 for the whole system and about the point O_2' for block 2, the final relations for transition to pattern 1a are

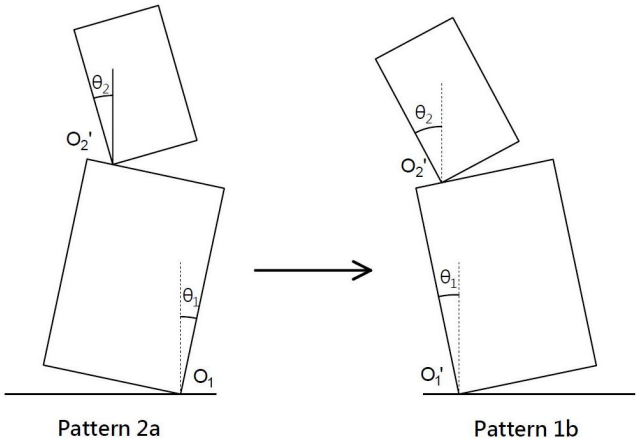

Fig. 2.17: Transition from pattern 2a to pattern 1b

$$\begin{aligned} \dot{\theta}_1^+ &= A\dot{\theta}_1^- + B\dot{\theta}_2^- \\ \dot{\theta}_2^+ &= C\dot{\theta}_1^- + D\dot{\theta}_2^- \end{aligned} \tag{2.81}$$

where

$$A = \frac{E_1E_2 - E_1E_3}{E_4E_1 - E_1E_5}; \quad B = \frac{E_1E_6 - E_7E_1}{E_4E_1 - E_1E_5}$$
$$C = \frac{E_5E_2 - E_4E_3}{E_1E_5 - E_1E_4}; \quad D = \frac{E_5E_6 - E_4E_7}{E_1E_5 - E_1E_4}$$

with

$$\begin{aligned} E_1 &= I_{O_2} \\ E_2 &= I_{O_1} + m_2 l' r \sin(\Theta - \beta' + \theta_1) \\ E_3 &= m_2 R_2 l' \cos(\theta_{C_2} - \beta' + \theta_1 - \theta_2) \\ E_4 &= I_{O_1} + m_2 l r \sin(\Theta - \beta + \theta_1) \\ E_5 &= m_2 R_2 l \cos(\theta_{C_2} - \beta + \theta_1 - \theta_2) \\ E_6 &= I_{C_2} + m_2 R_2 r \sin(\theta_{C_2} + \Theta + \theta_2) \\ E_7 &= I_{C_2} + m_2 R_2^2 \cos(\theta_{C_2} + \beta' - \theta_1 - \theta_2) \\ &. \end{aligned}$$

If the above equations lead to physically impossible case where $\dot{\theta}_2^+ < \dot{\theta}_1^+$, the block 2 remains attached to block 1 and the system rocks in pattern 3a. In that case

$$\dot{\theta}_1^+ = \dot{\theta}_2^+ = \frac{A_1}{I_o}\dot{\theta}_1^- + \frac{A_2}{I_o}\dot{\theta}_2^- \tag{2.82}$$

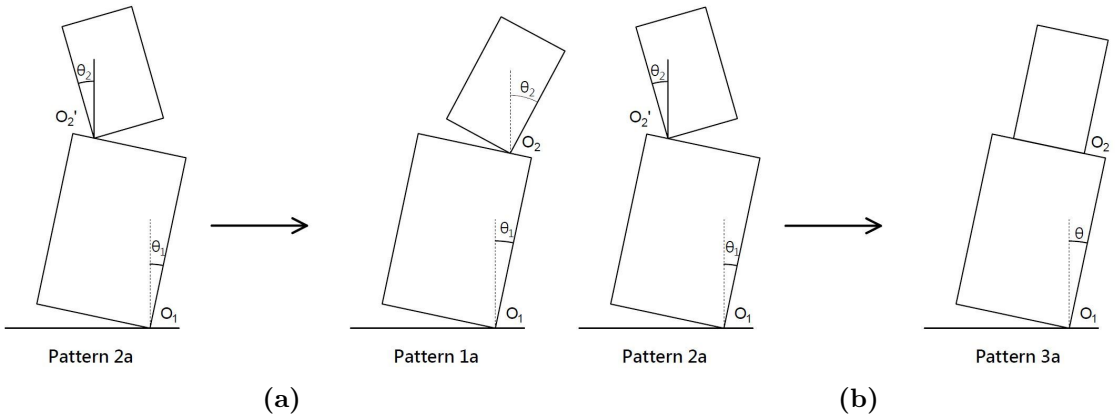

Fig. 2.18: Transition from pattern 2a to pattern 1a or to pattern 3a

where

$$A_1 = I_{O_1} + m_2 l' r \sin(\Theta - \beta' + \theta_1)$$
$$A_2 = I_{C_2} + m_2 R_2 r \sin(\theta_{C_2} + \Theta + \theta_2)\,.$$

The same equations also hold for the case of transition from pattern 2b to pattern 1b or to pattern 3a [24].

5. **Transition from pattern 3a to pattern 1b or to pattern 3b**
Assume the system is rocking in pattern 3a. When the impact occurs at point O_1' the block 1 starts rocking about this point. If the impact is strong enough, block 2 uplifts from block 1 and the system switches to pattern 1b as shown in Figure 2.19a. Otherwise block 2 remains in contact with block 1 so that the system rocks in pattern 3b, see Figure 2.19b. In the first case, from the conservation of angular momentum about the point O_1 for the whole system and about the point O_2' for block 2, one finds

$$\begin{aligned} \dot{\theta}_1^+ &= A\dot{\theta}_1^- \\ \dot{\theta}_2^+ &= B\dot{\theta}_1^- \end{aligned} \tag{2.83}$$

in which

$$A = \frac{C_1C_2 - C_3C_4}{C_5C_1 - C_3C_6}; \quad B = \frac{C_6C_2 - C_5C_4}{C_3C_6 - C_1C_5}$$

where

$$
\begin{aligned}
C_1 &= I_{O_2} \\
C_2 &= I_{O_1} - 2mb_1^2 \\
C_3 &= I_{C_1} + m_2 R_2[b_1 \sin\theta_{C_2} + (2h_1 + h_2)\cos\theta_{C_2}] \\
C_4 &= I_{O_1} + m_2 l'(h_2 \cos\beta' - b_2 \sin\beta') \\
C_5 &= I_{O_1} + m_2 l[(2h_1 + h_2)\cos\beta + b_1 \sin\beta] \\
C_6 &= m_2 l(h_2 \cos\beta + b_2 \sin\beta)
\end{aligned}
$$

.

If, however, the above equations leads $\dot{\theta}_2^+ > \dot{\theta}_1^+$, which is physically impossible, block 2 remains attached to block 1 after the impact. In that case, system moves as one rigid body (pattern 3a). Namely, $\dot{\theta}_2^+ = \dot{\theta}_1^+$ and the value of the angular velocity after the impact, derived from conservation of angular momentum about O_1', is

$$\dot{\theta}_1^+ = \dot{\theta}_2^+ = \left(\frac{I_{O_1} - 2mb_1^2}{I_{O_1}}\right)\dot{\theta}_1^- \,. \tag{2.84}$$

The above equations also hold for the case of transition from pattern 3b to pattern 1a or to pattern 3a [24].

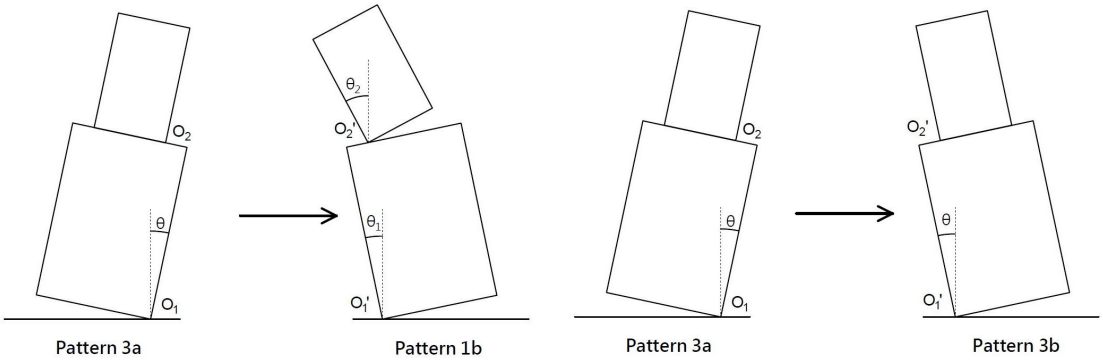

Fig. 2.19: Transition from pattern 3a to pattern 1b or to pattern 3b

6. **Transition from pattern 4a to pattern 1b or to pattern 4b**
   Lastly, let us consider the case where the system is rocking in pattern 4a. If θ_2 becomes zero, an impact with block 1 occurs. This usually leads to transition to pattern 4b although it is possible that pattern 1b is initiated. Two possibilities are illustrated in Figure 2.20. In latter case, the angular velocities after the impact, are expressed as

$$\begin{aligned}\dot{\theta}_1^+ &= A\dot{\theta}_1^- \\ \dot{\theta}_2^+ &= B\dot{\theta}_1^- + \dot{\theta}_2^-\end{aligned} \tag{2.85}$$

in which

$$A = \frac{C_1C_2 - C_3C_4}{C_5C_1 - C_3C_6}; \quad B = \frac{C_6C_2 - C_5C_4}{C_3C_6 - C_1C_5}$$

where

$$\begin{aligned}C_1 &= I_{O_2} \\ C_2 &= I_{C_2} + m_2R_2[(2h_1 + h_2)\cos\theta_{C_2} - b_1\sin\theta_{C_2}] \\ C_3 &= I_{C_2} + m_2R_2[(2h_1 + h_2)\cos\theta_{C_2} + b_1\sin\theta_{C_2}] \\ C_4 &= I_{O_2} - 2m_2b_2^2 \\ C_5 &= I_{O_1} + m_2l[(2h_1 + h_2)\cos\beta + b_1\sin\beta] \\ C_6 &= m_2l(h_2\cos\beta + b_2\sin\beta)\end{aligned}$$

If this analysis leads to $\dot{\theta}_1^+ > 0$, which is psychically impossible, block 1 remains still after the impact and only block 2 continues rocking (pattern 4b). In that case, $\dot{\theta}_2^+$ is

$$\dot{\theta}_2^+ = \left(\frac{I_{O_2} - 2m_2b_2^2}{I_{O_2}}\right)\dot{\theta}_2^- . \tag{2.86}$$

The same equations also hold for the case of transition from pattern 4b to pattern 1a or to pattern 4a [24].

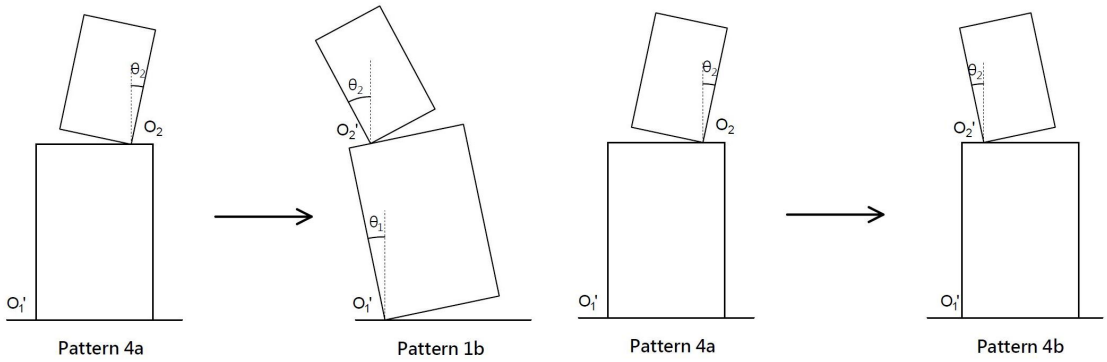

Fig. 2.20: Transition from pattern 4a to pattern 1b or to pattern 4b

2.3 The response spectrum vs. the rocking spectrum

In order to quantify the shaking potential of a earthquake, response spectrum can be used for SDOF oscillator and the rocking spectrum for the rocking block. Priestley et al. [16] assumed that "it is possible to represent a rocking block as a single-degree-of-freedom (SDOF) oscillator with constant damping" (e.g. linear, viscously damped oscillator), where the slenderness (θ_c) of the rocking block is a measure of the minimum damping of the system. Figure 2.21a shows the diagram of the two SDOF structures at deformed configurations when subjected to ground motion. The response quantities of interest in case of SDOF oscillator are its relative displacement, u, and its time derivatives. The corresponding quantieis of interest for the rocking block are its angle of rotation, θ, and its angular velocity, $\dot{\theta}$. In the first case the restoring mechanism originates from the elasticity of the structure, while the restoring mechanism of the rocking block originates from gravity. As can be seen from Figure 2.21a, representing the force-displacement and moment-rotation relations of the two structures of interest, the SDOF oscillator has a positive and finite stiffness, k, and energy is dissipated as the force-displacement curve forms a closed loops. On the other hand, the rocking block has an infinite stiffness until the magnitude of the applied moment reaches $mgR\sin\theta_c$, thereafter the stiffness is negative. Table 2.2 summarizes differences in dynamical structure of SDOF oscillator and rocking block. Because of these essential differences, any analogy between the response of these two systems tends to be superficial.

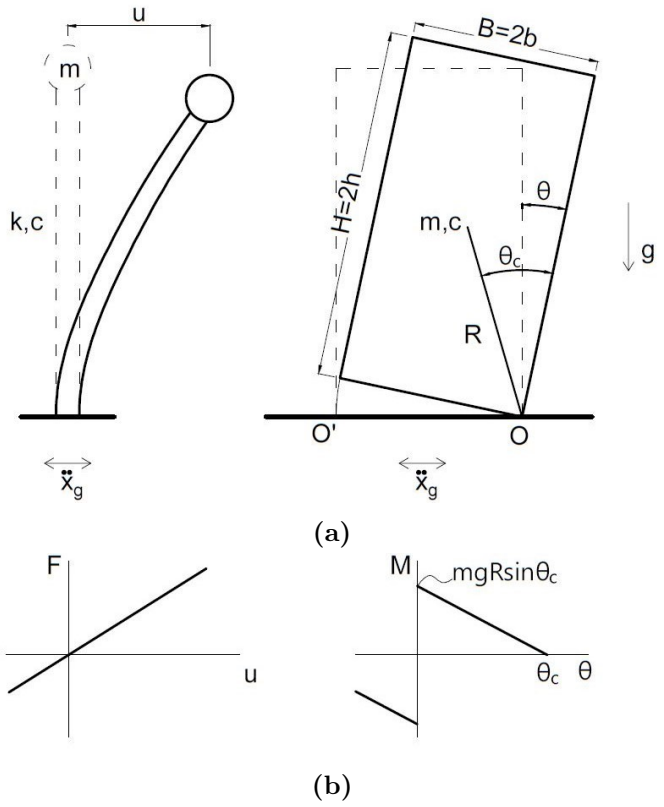

Fig. 2.21: (a)Schematic of a SDOF oscillator (left) and of a rocking block (right) in motion; (b)Corresponding force-displacement (left) and moment-rotation diagram

Tab. 2.2: Selective characteristics and parameters of the two SDOF system of interest

System	Damped oscillator	Rocking rigid block
Parameters/characteristics	m, c, k	b, h, g
Restoring mechanism	Elasticity of the structure	Gravity
Restoring force/moment	$F = ku$ (for linear springs)	$M = mgR\sin(\theta_c - \theta)$
Restoring force/moment at stable equilibrium	Zero	Finite: $mgR\sin\theta_c$
Stiffness at stable equilibrium	Finite	Infinite
Stiffness away from equilibrium	Positive	Negative
Frequency parameter	Undamped natural frequency: $\omega_o = \frac{2\pi}{T_o} = \sqrt{\frac{k}{m}}$	Frequency parameter: $p = \sqrt{\frac{3g}{4R}}$ (for rectengular blocks)
Damping parameter	Viscous damping ratio: $\xi = \frac{c}{2m\omega_o}$	Slenderness: $\theta_c = \tan^{-1}(b/h)$

The response spectrum plots the response maxima as a function of the natural period of the SDOF oscillator, $T_o = 2\pi/\omega_o$, and the viscous damping ratio, ξ. On the other hand the rocking spectrum shows plots of the maximum rotation, θ, and maximum angular velocity, $\dot{\theta}$, versus the inverse of the frequency parameter of the geometrical similar blocks (i.e. with same H/B ration). Makris and Konstantinidis [20] shows in his work several examples of the response and rocking spectrum for different earthquake motions. Observing these examples one can notice that the displacements of the linear, viscously damped oscillator increase as natural period increases and after reaching a maximum converge to the ground displacement. However, the rotations of the rocking block decrease nearly monotonically with an increase in its apparent "period", $T = 2\pi/p$. Further there are period ranges where the displacement values are nearly insensitive to the value of viscous damping ratio. Contrarily, the rotation spectrum is very sensitive to the value of block slenderness through the $2\pi/p$. Also, if a response spectrum of one earthquake exceeds the response spectrum of another earthquake, for a specific value of viscous damping, same relation will be observed (with few local exceptions) for a different value of viscous damping. However, if the rocking spectrum of one earthquake exceeds the rocking spectrum of another earthquake, it is not necessarily that the same relation will happen for a slightly different value of the slenderness.

In a view of these differences, the response spectrum of SDOF oscillator should not be used to draw conclusions or approximate the response of the rocking block. Rather the rocking spectrum can be used as a complimentary tool to the response spectrum in order to quantify the shaking potential of a ground motion [20].

Chapter 3

Details of the shake table test program

3.1 Design and characteristics of the experimental specimens

The experimental model was designed while considering three conditions. Firstly, it is sufficiently stiff to be considered as rigid blocks. Secondly, there should be no sliding between two blocks or the block and the base. The last criteria says that the impact occurs only in corner edges, i.e. the only pivotal points are corner edges of the blocks. The main motivation for this study and a significant example of this class of structures are the statues and the statue-pedestal system. Those are commonly found on the ground floor of museums or in the area outside of museums. For that reason ground earthquake motions are used in this study. Other free standing, unattached objects, e.g. shelves and medical equipment, can be found on the upper floors of the buildings as well. In effort to include such scenarios in the study, earthquake responses on 3rd and 5th floor were derived from the ground motions.

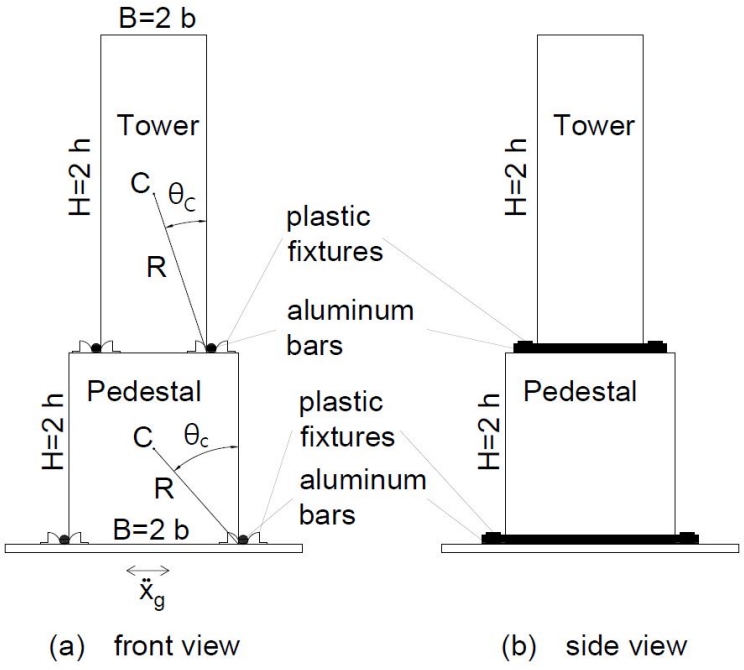

Fig. 3.1: Schematic of tower-pedestal system

The size of blocks, glued from lacquered 19 mm thin MDF plates, was determined such that small disturbances, like an attachment of pickups and accelerometers would not affect their behavior considerably. The solid, composite material the blocks were made of, is the reason why they can be considered as rigid blocks. In order to insure pure rocking, aluminum round bars were attached on the sides of the block. In this way pivotal points are clearly defined. A schematic of the dual body system is presented in Figure 3.1, whereas the photos of physical models along with its key dimensions are shown in Figure 3.2. The geometric and mass properties of each block are included in Table 3.1. The height of the top blocks, representing statues, T_1, T_2

Tab. 3.1: Characteristics of the individual test specimens

Block Specimen	$2b$ [cm]	$2h$ [cm]	m [g]	θ_c [rad]	R [cm]	p [s^{-1}]	H/B [-]
T_1	12.4	37.2	2172	0.322	19.61	6.13	3
T_2	12.4	49.6	2790	0.245	25.56	5.36	4
T_3	12.4	62.0	3456	0.197	31.61	4.82	5
P	18.4	20.8	2300	0.724	13.89	7.28	1.13

$\theta_c = \cot^{-1}(h/b)$; $R = \sqrt{b^2 + h^2}$; $p = \sqrt{3g/4R}$

and T_3 were fixed to achieve a height-width ratio, i.e. slenderness, of $3, 4$ and 5, respectively, with width equal to $12, 4$cm, representing slender blocks. The notation T stands for tower. The bottom block is more squat with slenderness of 1.13. It represents the pedestal, therefore the notation P.

3.2 Test setup

Experimental tests were carried out on the uni-axial shaker system Wolfel BD.5. The shaker is force guided by electrodynamic drive. It's maximal stroke is 290mm for frequency range from 0.5 to 200Hz depending on the reaction mass. The shaker's maximum input force is 500N. For the purpose of this study the shaker was set horizontally with attached wooden plate, as can be seen in Figure 3.3a. The shaker itself was fixed to the concrete blocks and two U steel beams in order to ensure its stability. Further, specially designed fixtures, made of plastic, were attached on the wooden plate as well as on the bottom block, P. These fixtures serve as a support for the aforementioned aluminum bars and ensure that any other motion except rocking is excluded. Furthermore, the upper block is secured by a safety cable, in order to prevent its downfall and to avoid any damages to the instruments or the blocks in case of block overturning. It is noted that the length of the cable was sufficient so it won't interfere with the rocking motion.

In this study both single block system, i.e. towers without the pedestal, as well as two blocks configurations, i.e. towers atop the pedestal were tested. Table 3.2 summarizes the tested combinations. Before each test run, the contact surfaces between the block and the wooden plate as well as between the blocks in case of two-body system are cleaned from the dust. Furthermore, it was made sure that the joints are good positioned and firmly fixed to the wooden plate. During

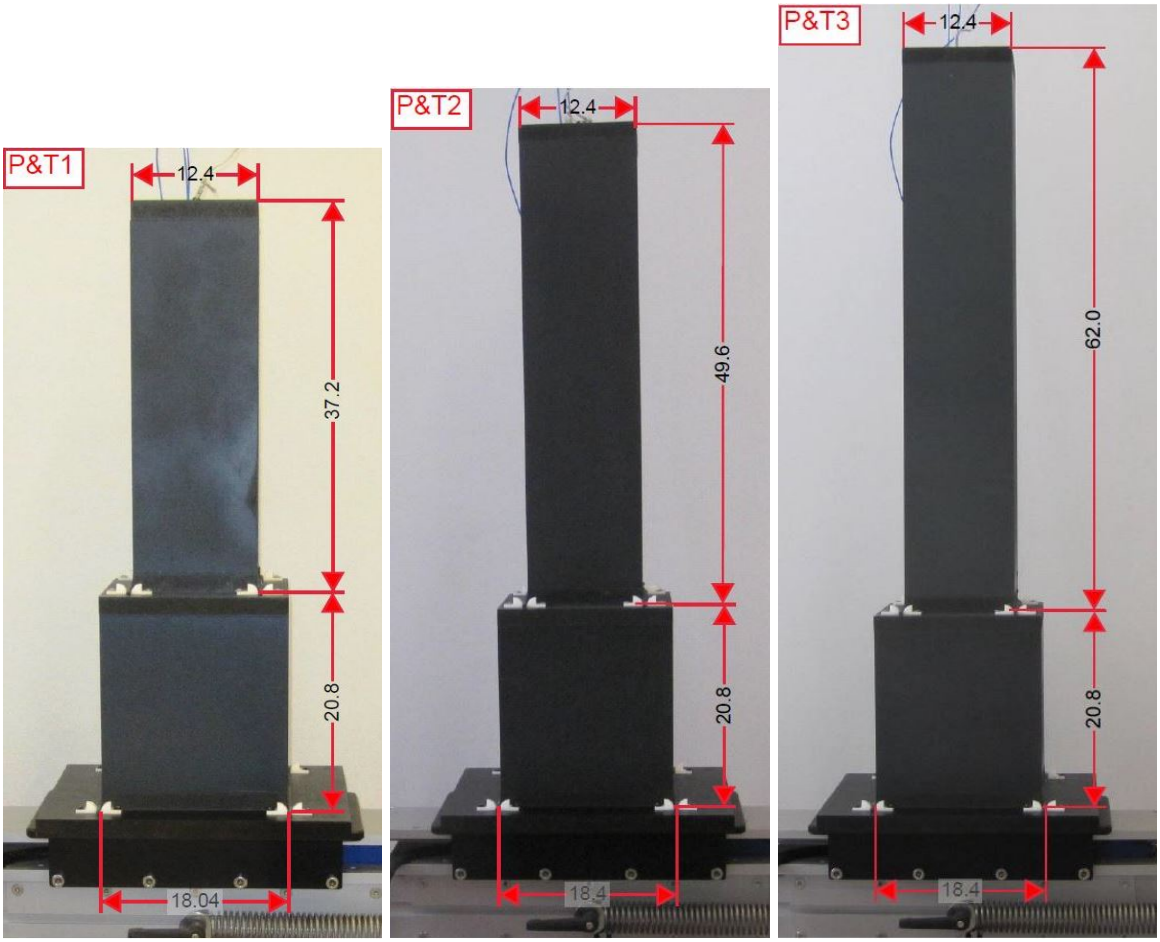

Fig. 3.2: Physical model of the tower-pedestal system with its key dimensions. Note:All units in centimeters

Tab. 3.2: List of tested configurations

No.	Name	Pedestal	Tower block
1	T_1	n/s	T_1
2	T_2	n/s	T_2
3	T_3	n/s	T_3
4	$P\&T_1$	P	T_1
5	$P\&T_2$	P	T_2
6	$P\&T_1$	P	T_3

each test shaker driven force was gradually increased until one of the blocks overturns. The maximal accelerations are then calculated in the processing phase.

3.3 Selected input earthquake motion

The specimens were expected to have good durability and almost none damage accumulation during the shake table tests. Because of that, the only limitation to the number of input motions

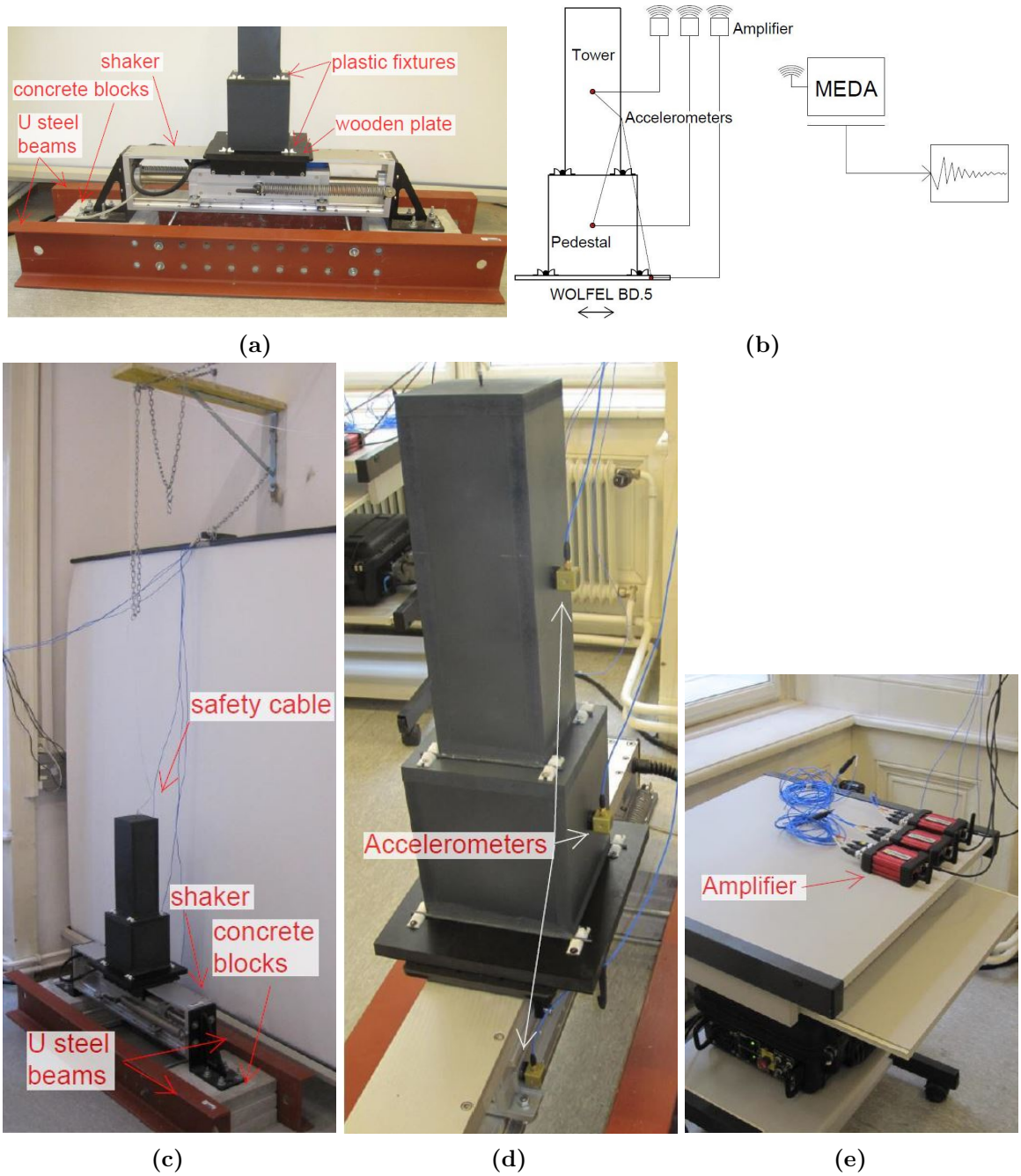

Fig. 3.3: Test setup (a) front view; (b) schematics; (c) angle view; (d) side view; (e) amplifiers

and test repetitions was time requiared to run the tests. For this study four earthquake events were chosen. Namely, 1976 Friuli, 1995 Kobe, 1989 Loma Prieta and 1994 Northridge. In order to observe behavior of structures inside the building and not just on the ground, for each earthquake event the response on 3rd and 5th floor of a masonry building, i.e. the acceleration time history for these floors, were derived [27]. In this way, each specimen was subjected to 12 different input motions. Selected ground motions are shown in table 3.3, along with the acceleration time history of the ground motions depicted in Figure 3.4.

Tab. 3.3: Ground motions used in this study

Date-Earthquake	Mw	PGA[1] [g]	PGV[1] [cm/s]	PGD[1] [cm]
06/05/1976 - Friuli, Italy	6.5	0.35	22.02	4.07
17/01/1995 - Kobe, Japan	6.9	0.34	27.68	9.69
17/10/1989 - Loma Prieta	6.9	0.37	44.70	19.61
17/01/1994 - Northridge	6.7	0.57	52.01	9.03

[1] PGA-peak ground acceleration; PGV-peak ground velocity; PGD-peak ground displacement

The Friuli earthquake of a magnitude of 6.5(M_w) occurred on May 6 1976 in the central Friuli region, located in the northeast Italy at the borders of the Austria and Slovenia. Large number of schools, churches, town halls and factories were destroyed. In addition Renaissance castles, other historical landmarks and important art treasures were damaged causing loss to architectural and cultural heritage.

The 1995 Kobe earthquake hit the southern part of Hyogo prefecture on Jan 17. It registered as a 6.9 on the moment magnitude scale. It caused several thousands casualties. The damage was severe and widespread. Many building and old houses were destroyed. Numerous elevated roads and bridges also suffered irreparably damage.

The Loma Prieta earthquake occurred in San Francisco Bay Area of California on Oct 17. It measured 6.9 on the moment magnitude scale. During the earthquake double deck portion of the Cypress Street Viaduct on Nimitz Freeway collapsed, crashing the cars on the lower deck and causing numerous fatalities. Also San Francisco-Bay bridge collapsed. Among the many buildings that were damaged, was Oakland City Hall and Pacific Garden Mall in Santa Cruz.

The 1994 Northridge earthquake with a magnitude of 6.7(M_w) was a blind thrust earthquake, that happened on Jan 17. It was centered under the community of the Northridge, in San Fernando Valley region of the county of Los Angles. It's example of broad brand ground motion. Even though it wasn't the most energetic it caused severe damaged, because it occurred in a urban area. Many of two and three story buildings suffered partial or total collapse. Couple large parking structures and bridges collapsed or were severely damaged.

3.4 Instrumentation and data processing

To monitor the response of the shake table and dual body system, PCB-356B18 accelerometers were used, with a range $\pm 5g$ and frequency up to 30000Hz. The acceleration was recorded on the surface of the shake table, as well as at the mid-height of each block, as can be seen from the position of the accelerometers in Figure 3.3. These are tree-axial piezoelectric accelerometers..

A piezoelectric accelerometer is a device that uses piezoelectric effect in order to measure dynamic acceleration of an object as a function of voltage. Piezoelectric effect is the ability present in certain materials to generate electric charges when mechanical stress is applied on them. This effect occurs due to shifting of the centers of positive and negative electric charges in

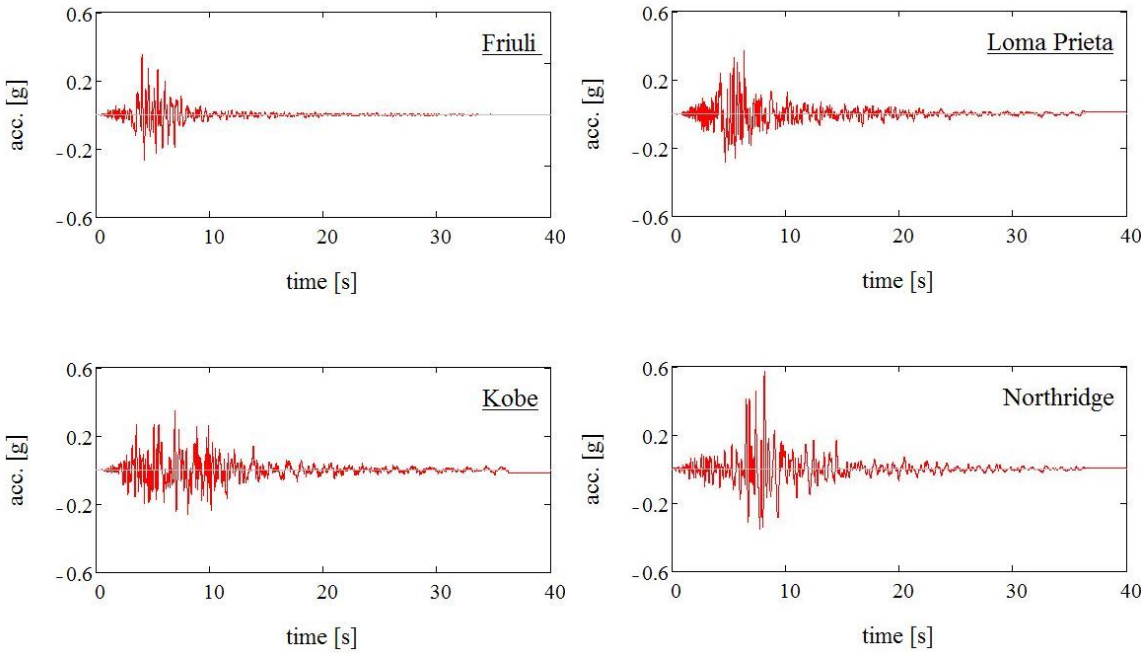

Fig. 3.4: Acceleration time historys of input ground motions

a material which suffers under mechanical stress. Furthermore, this scenario leads to external electrical field.

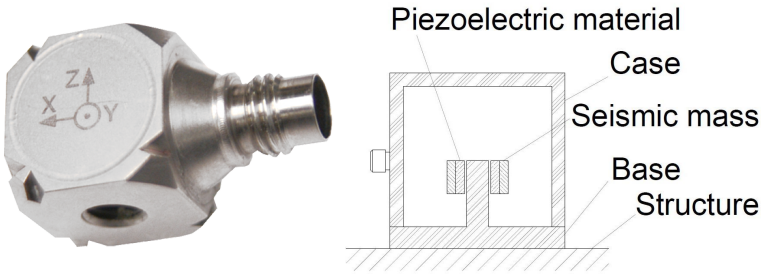

(a) **(b)**

Fig. 3.5: (a) Piezoelectric accelerometer [28] ; (b) Schematic cross sectional view

When the observed object is moving, dynamic acceleration is transmitted to a seismic mass, which is positioned inside the accelerometers. The seismic mass is bonded to the structure of the sensor by piezoelectric material (Figure 3.5). Dynamic acceleration of the seismic mass generates mechanical stress on the piezoelectric material, which results in high-impedance electrical charge proportional to the applied force and therefore, proportional to the acceleration of the object.

The main advantages of using piezoelectric accelerometer are:

- High frequency response: parameters changing at high velocities can be sensed

- High transient response: short-termed events can be detected while linearity of the signal conserved
- Small size of the sensor and robustness of the construction.

Accelerometers were connected through wires to the signal amplifiers. These send the signal to a receiver connected to a computer. Further, a software MEDA was used for processing the data. The schematic of the system is depicted in Figure 3.3b, along with the pictures of system (Figure 3.3d and 3.3e). The data captured by the accelerometers were used in post-processing to verify the accuracy of calculated maximum acceleration, that the system achieves, just before overturning. Namely, the maximum accelerations were calculated based on shaker input force and the reaction mass, i.e. the weight of the blocks.

Chapter 4

Results and interpretation of earthquake tests

4.1 Initiation of motion

In this study rocking of configurations shown in Table 3.2 was observed, i.e. single body and two-body configurations. Minimum ground acceleration needed to initiate rocking, in further text initial acceleration, was calculated based on simple statics and physics relationships as defined in equations 2.1 and 2.21 - 2.25 and presented in Table 4.1. T_1, T_2 and T_3 single rocking blocks, whereas $P\&T_1, P\&T_2$ and $P\&T_3$ are dual-body systems. Patterns 3 and 4 reflect SDOF system response. In particular, pattern 3 describes the motion of the system rocking as one rigid structure, and pattern 4 concerns the case where only the top block experience rotation. The bottom part of Table 3.2 includes initial acceleration for stacked configurations. It shows that smaller value is needed to initiate rocking in pattern 4 compared to pattern 3. Because in the pattern 4 only the top block is rocking, it's not surprising that the initial acceleration is the same as in the case of the single block system. Thus, higher excitation is needed to induce rocking in both blocks in case of two block assemblies compared to single block. Further it can be noticed that with the increase in block slenderness, the initial acceleration decreases, meaning that more slender blocks are more prone to start rocking then the squatter ones.

Tab. 4.1: Initiation of rocking

System	$min\ \ddot{x}_g[\mathrm{m/s^2}]$	
T_1	3.27	
T_2	2.45	
T_3	1.96	
	Pattern 3	Pattern 4
$P\&T_1$	3.69	3.27
$P\&T_2$	3.04	2.45
$P\&T_3$	2.56	1.96

4.2 Effect of tower geometry

To investigate the effect of the tower geometry on stability of the system, the maximum achieved horizontal acceleration of each tower configuration with various slenderness is included in

Figure 4.1. The plots include tower configuration both without the pedestal and with the pedestal. Further, the mean value is overlaid on each plot in order to assist in trend identification. As can be seen from these plots, the overturning acceleration decreases almost linearly with the increase of the slenderness. In other words squatter blocks are more resistant to ground shaking. The same trend is noticeable in both plots, without and with the pedestal. Furthermore, the relative decrease of the mean value is nearly the same for single and stacked configuration. Same tendencies can be observed if we look at the data from each floor separately for one block system as well as for two block system depicted in Figure 4.2. Unlike the previous plots, the data in these plots show different relative decrease both for separate floors and for presence of the pedestal.

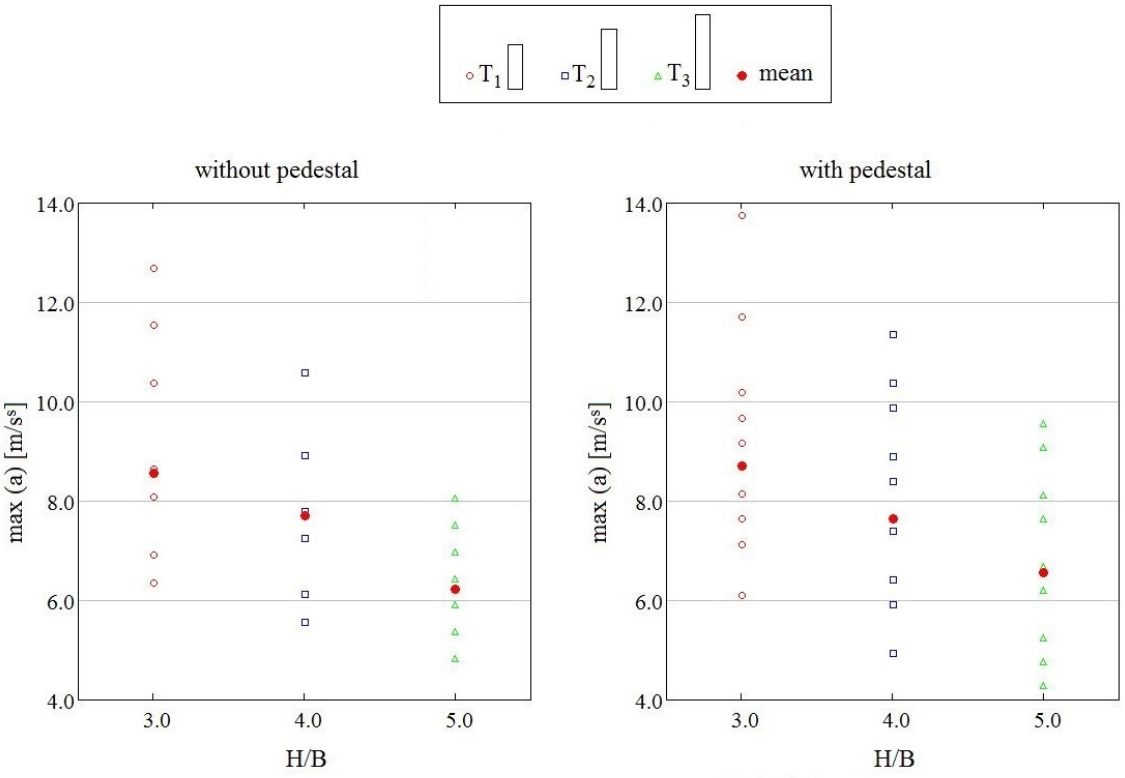

Fig. 4.1: Scatter plots of maximum system acceleration for each of three tower geometries

4.3 Effect of pedestal

In order to study effect of presence of the pedestal on the system resistance, maximum achieved acceleration of the system without pedestal are plotted against the system with pedestal in Figure 4.3. The data markers correspond to the tower configuration, where on x-axes are the values of configurations without the pedestal and on y-axes the values of stacked configurations. In addition to this, 1-to-1 line was added to aid in interpretation of the results The main observation is the trend of higher maximum acceleration in case of pedestal presence.

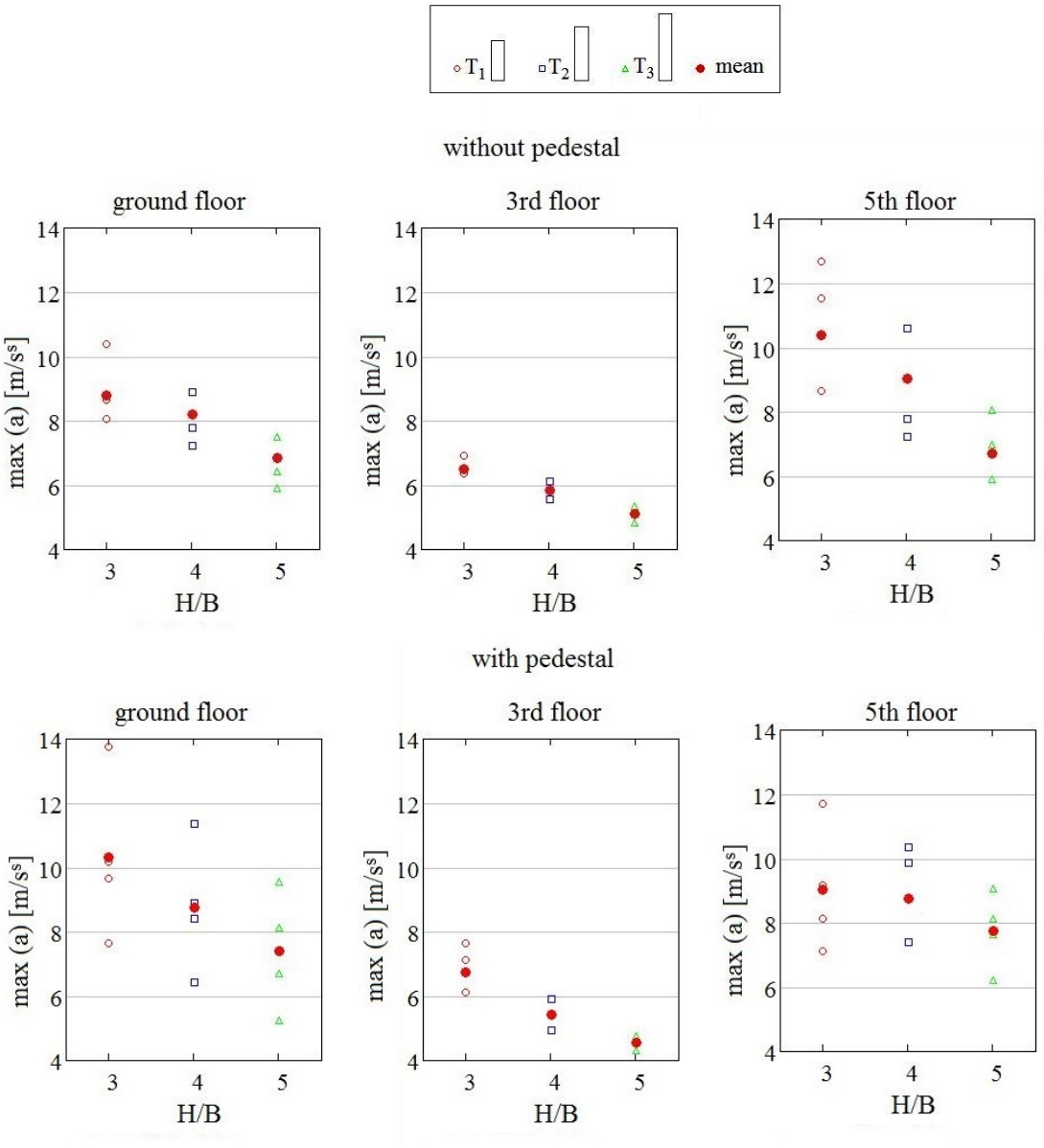

Fig. 4.2: Scatter plots of maximum achieved acceleration for individual floor and for each of three tower geometries

The presence of the pedestal, the combined center of two blocks raises vertically and makes the whole structure more slender. Despite this fact and the aforementioned fact that smaller acceleration is needed to overturn the more slender structure, the system with pedestal can endure higher acceleration before overturning. To further verify this conclusion, the maximum acceleration was plotted in accordance to the slenderness and the presence of the pedestal, in Figure 4.4. The corresponding mean values are included as well. The degree of increase in mean value of maximum achieved acceleration, in case of presence of the pedestal shows no correlation to the slenderness. The increase is most significant for the T_3 tower. The presence of the pedestal has nearly opposite effect for T_2 tower, however the slight increase is still evident.

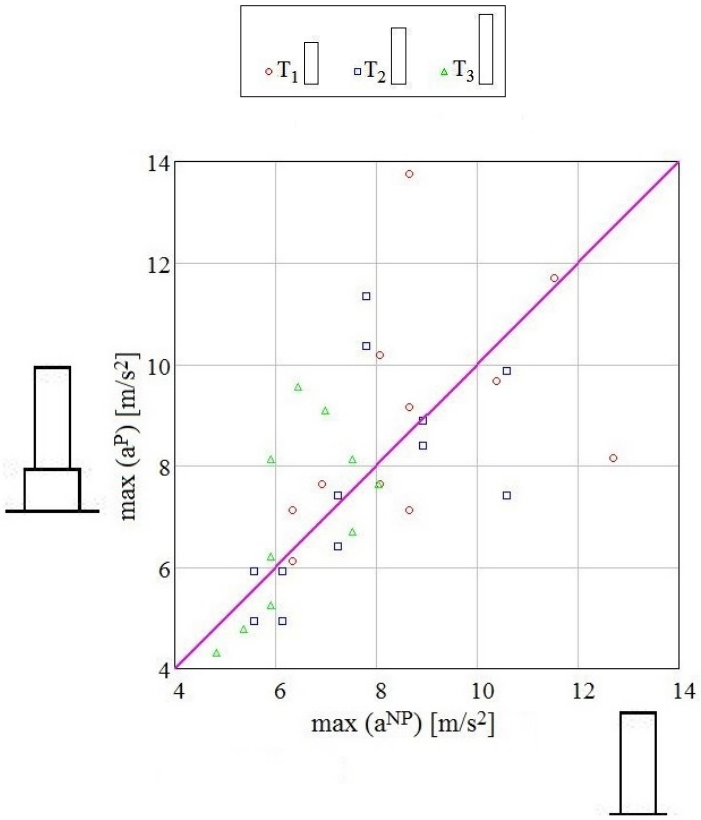

Fig. 4.3: Scatter plot of maximum system acceleration for individual tower geometries atop the pedestal ('P') versus that as a single body ('NP')

On the other hand, from the plots shown in Figure 4.6, depicting different maximum acceleration in accordance to the floor and presence of pedestal, the increase in maximum acceleration in case of presence of the pedestal is only noticeable on the ground floor. Stacked configuration does not lead to the same behavior for the 3rd and 5th floor, rather the maximum achieved acceleration slightly decreases with the presence of the pedestal. If each tower is further separately investigated, as shown in Figure 4.6b, the same trends can be observed, with exception of the Tower 1 on the 3rd floor. Namely, for the Tower 1 an increase in the maximum acceleration, in case that the pedestal is present, in noticeable on the 3rd floor. Further it can be concluded that increase of the maximum acceleration on ground floor as well decrease on 5th floor the the Tower 1 is much greater than for other two tower geometries.

4.4 Effect of input motion

In this section two scenarios are going to be discussed: how does the system behave on different floors on one hand, and on another its behavior in case of different earthquake events. A set of scatter plots for each floor separately is presented in Figure 4.5. The data markers indicate the tower configuration, and the presence of the pedestal is defined along the $x-$ (without pedestal)

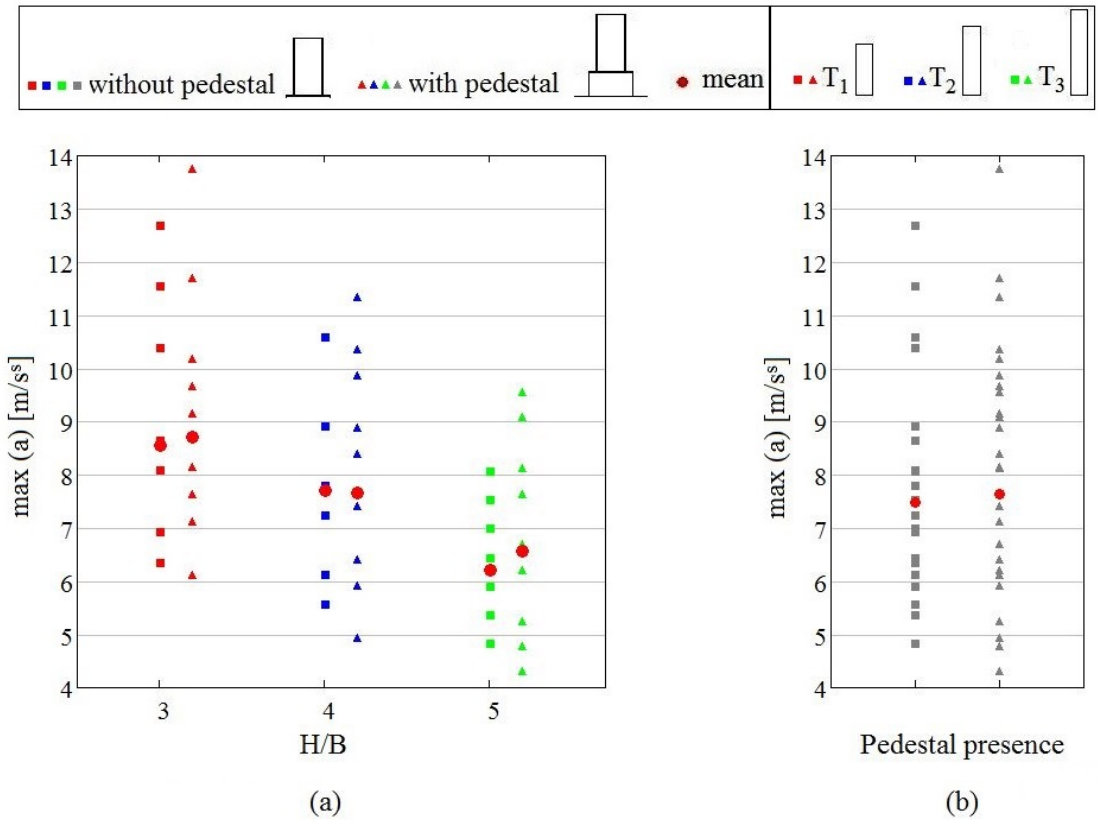

Fig. 4.4: Scatter plots of maximum system acceleration for (a) each of three tower geometries and (b) all tower geometries and presence of the pedestal

and $y-$ (with pedestal) axis. As previously presented depending on for which floor is the input motion tested, the presence of the pedestal may increase (for ground floor) or decrease (for 3rd and 5th floor) the maximum achieved acceleration as seen in Figure 4.6 and 4.5. The only anomaly in this pattern is the response of Tower 1 for 3rd floor. The relative change is the most noticeable on the ground floor.

It is interesting to note that, the maximum achieved acceleration is smallest for the 3rd floor in comparison to the ground and 5th floor regardless of the tower geometry and presence of the pedestal. The tested configurations reach the maximal mean value, of the maximum achieved acceleration, on the 5th floor in case of a dual body system. However for the configurations without the pedestal the maximum achieved acceleration is on the ground floor.

The plots presented in Figure 4.7 show the maximum achieved acceleration of the tower atop a pedestal plotted against the tower without the pedestal for different earthquake events. In these plots, the data markers correspond to different tower configurations (i.e. T_1, T_2, T_3). In these cases it is easy noticeable that the configuration with the pedestal can endure greater accelerations before overturning. That is not the case just in the event of 1994, Northridge earthquake where the towers with the pedestal overturn under smaller excitation that the one

with the pedestal, but also for other tested earthquake motions. The increase in overturning acceleration is the most distinguished in case of 1989, Loma Prieta earthquake.

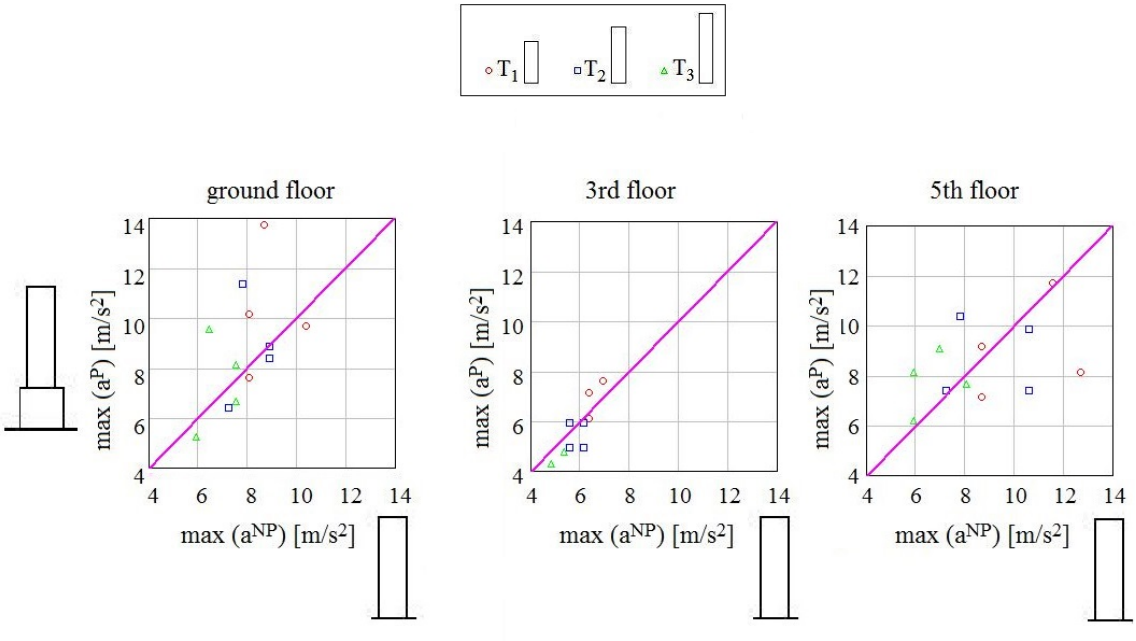

Fig. 4.5: Scatter plots of maximum acceleration for individual floors events and tower configuration atop the pedestal ('P') versus that as a single body ('NP')

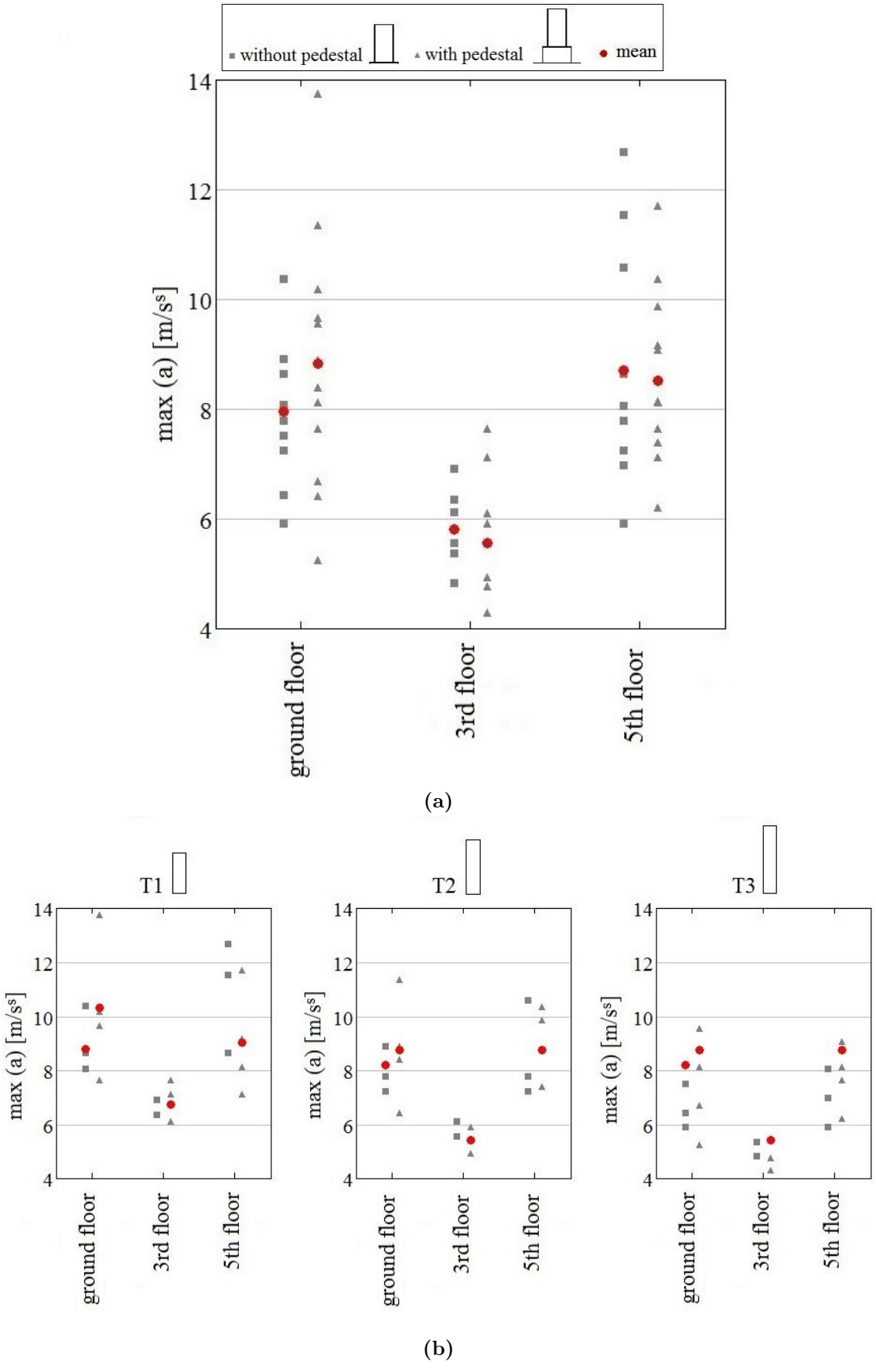

Fig. 4.6: Scatter plots of maximum achieved acceleration for each floor and presence of the pedestal for (a) all tower configurations and (b) each tower separately

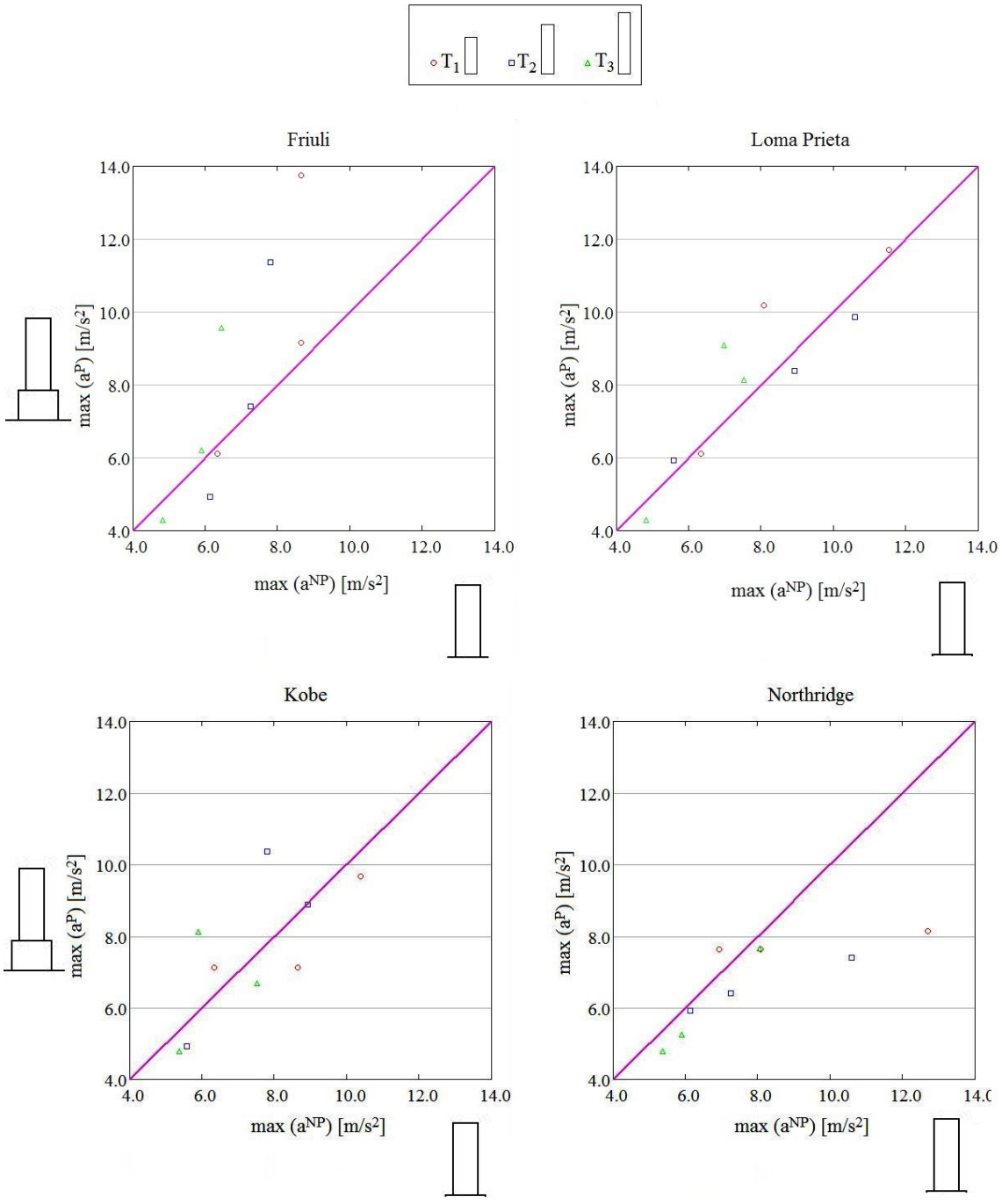

Fig. 4.7: Scatter plots of maximum acceleration for individual earthquake events and tower configuration atop the pedestal ('P') versus that as a single body ('NP')

Chapter 5

Conlusions and future work

Systems of unattached, stiff, freestanding, single, or multiple bodies are highly susceptible to damage and overturning in the case of an earthquake, as evidenced in numerous earthquake events. In an effort to better understand and to gain the possibility to predict behavior of these structures, data from shake table experiments are necessary. In order to complement the limited experimental database, shake table testing campaign is conducted on wooden blocks. The height to width ratio of the blocks varies from 1.13 through 5. The slender blocks ($H/B \geq 3$)), were tested both as a single body, and in a stacked configuration with a squat pedestal ($H/B = 1.13$). In total, 6 different configurations were tested on the uni-axial shaker system. This geometric range and presence of the pedestal may be used to understand response of statues, as well as electrical transformers, office, medical, and other equipment. The configurations were tested using not just recorded earthquake motions, but its simulated motion on the 3rd and 5th floor, in order to understand the dynamic behavior of the structures in the building as well as on the ground. The rocking response of each specimen was recorded in time and maximum achieved acceleration was obtained in an effort to correlate the tower geometry and the presence of the pedestal with rocking endurance.

In general, tower configurations were observed to be more stable atop the pedestal than in the single-block configuration. However, when each floor was examined separately, the maximum achieved acceleration decreases, with a few exceptions, with the presence of the pedestal on the 3rd and 5th floor. This decrease is slight, and therefore should be taken with caution, whereas the increase on the ground floor was significant. Further tests are suggested in order to confirm and explain this behavior.

The maximum achieved acceleration is significantly increased with the presence of a pedestal in the case of Friuli earthquake input motion. The increse in maximum achieved acceleration is observed to a much smaller degree for Loma Prieta and Kobe input motion, however it was still evident. On the other hand, Northridge input motion had the opposite effect, in that the configurations of the tower without the pedestal achieved greater maximum acceleration than in stacked configuration. The correlation between the input motion characteristic and the rocking response of specimens couldn't be found, therefore further investigation with more input motions is advised.

The results of this experiment reveal the dependence of the tower slenderness on the magnitude of its rocking response. Namely, more slender structures overturn under smaller excitation than squatter ones. This trend is visible in configuration with, as well as without a pedestal.

Due to the high sensitivity of response of the freestanding structures to changes in specimens geometry, the idea of extrapolating observed trends for other geometries should be considered carefully. It is possible to extended the current experiment on other tower geometries with different slenderness, as well as on the same slenderness but using different sizes. Furthermore, the other pedestal configurations could be included, in an effort to further understand the influence of the pedestal presence on the rocking response. The other input motions, e.g. single and multiple impulse motion, sinusoidal motions, and other recorded earthquake motions should also be considered. In this way, response data base would be enlarged and system parameters for possible systematic trends could be identified.

Bibliography

[1] N. T. K. Lam and E. F. Gad. "Overturning of non-ctructural components in low-moderate seismicity". In: *Earthquake Engineering in the low and moderate seimic regions of Southeast Asia and Australia* Special Issue (2008), pp. 121–132.

[2] E. Santimano. *Temple of Athena Aphaia, Aegina Islands, Greece.* 2004. URL: `https://www.flickr.com/photos/eustaquio/3010347082/in/photostream/` (accessed 02/18/2019).

[3] D. Konstantinidis and N. Makris. "Sesmic response analysis of multidrum classical columns". In: *Earthqauke Engineering and Structural Dynamics* 34 (2005), pp. 1243–1270.

[4] Y. Ishiyama. "Motions of rigid bodies and crieteria for overturning by earthquake excitation". In: *Earthquake Engineering and Structural Dynamics* 10 (1982), pp. 635–650.

[5] J. Milne. "Experiments in observational seismology". In: *Transactions Seismological Society Japan* 3 (1881), pp. 12–64.

[6] J. Perry. "Note on the rocking of a column". In: *Transactions Seismological Society Japan* 3 (1881), pp. 103–106.

[7] G. W. Housner. "The behaviour of inverted pendulum structures". In: *Bulletin of the Seismological Society of America* 53 (1963), pp. 403–417.

[8] W. Eppensteiner. URL: `https://www.zamg.ac.at/cms/de/images/geophysik/nachrichten/universitaet-wien-1` (accessed 03/07/2019).

[9] *The Earthquake of 1906: Stanford University and Environs.* URL: `https://library.stanford.edu/spc/exhibitspublications/past-exhibits/earthquake-1906-stanford-university-and-environs` (accessed 03/07/2019).

[10] MRPEngineering. "Sesmic Restraint for Equipment". In: *MRP Engineering Newsletter, Bellevue, WA* (2013).

[11] FEMA. "Reducing the Risk of Nonstructural Earthquake Damage - A Practical Guide". In: *FEMA E-74, Waschington, D.C.* (2011).

[12] *California wine country hit by strong 6.0-magnitude quake.* URL: `https://www.straitstimes.com/world/americas/california-wine-country-hit-by-strong-60-magnitude-quake` (accessed 03/07/2019).

[13] N. Makris and C. Black. "Uplifting and Overturning of Equipment Anchored to a Base Foundation". In: *Earthquake Spectra - EARTHQ SPECTRA* 18 (2002).

[14] M. Aslam, W. G. Godden, and D. T. Scalise. *Earthquake rocking response of rigid bodies*. report No.LBL-7539. Lawrence Berkeley Labaratory,University of California, Berkly, California, 1978. 35 pp.

[15] C.-S. Yim, A. K. Chopra, and J. Penzien. "Rocking response of rigid blocks to earthquakes". In: *Earthquake Engineering and Structural Dynamics* 8 (1980), pp. 565–587.

[16] M. J. N. Priestley, R. Evison, and A. Carr. "Seismic response of structures free to rock on their foundations". In: *Bulletin of the New Zeland National Society for Earthquake Engieneering* 11(3) (1978), pp. 141–150.

[17] P. D. Spanos and A.-S. Koh. "Rocking of rigid blocks due to harmonic shaking". In: *Journal of Enginering Mechanics* 110 (1984), pp. 1627–1642.

[18] W. K. Tsao and C. M. Wong. "Steady state rocking response of rigid blocks Part 1: Anlysis". In: *Earthquake Engineering and Structural Dynamics* 18 (1989), pp. 89–106.

[19] S. Hogan. "The many steady state responses of a rigid block under harmonic forcing". In: *Earthquake Engineering and Structural Dynamics* 19 (1990), pp. 1057–1071.

[20] N. Makris and D. Konstantinidis. "The rocking spectrum and the limitations of practical design methodologies". In: *Earthquake Enginering and Structural Dynamcis* 32 (2003), pp. 265–289.

[21] M. A. ElGawady, Q. Ma, J. W. Butterworth, and J. Ingham. "Effects of interface material on the performance of free rocking blocks". In: *Earthquake Enginering and Structural Dynamcis* 40 (2011), pp. 375–392.

[22] D. Kalliontzis, S. Sritharan, and A. Schultz. "Improved coefficient of restitution estimitation for free rocking members". In: *Journal of Structural Engineering* 142 (2016), p. 06016002. DOI: 10.1061/(ASCE)ST.1943-541X.0001598.

[23] I. N. Psycharis. "Dynamic behaviour of rocking two-block assemblies". In: *Earthquake Enginering and Structural Dynamcis* 19 (1990), pp. 555–575.

[24] P. D. Spanos, P. C. Roussis, and N. P. A. Politis. "Dynamic analysis of stacked rigid block". In: *Soil Dynamics and Earthquake Engineering* 21 (2001), pp. 559–578.

[25] A. N. Kounadis. "Rocking instability of free-standing statues atop slender cantilevers under ground motion". In: *Soil Dynamics and Earthquake Engineering* 48 (2013), pp. 294–305.

[26] P. C. Roussis. "Dynamic analysis of stacked rigid blocks". Master Thesis. Rice University, 1999.

[27] A. Rudisch. "Historic freestanding facade components under earthquake excitation". Dissertation. TU Wien in appraisal, 2018.

[28] URL: https://www.kistler.com/de/produkt/type-8688a/ (accessed 03/07/2019).